Chemical Science

ROYAL SOCIETY OF CHEMISTRY

REVIEW

View Article Online
View Journal | View Issue

Cite this: *Chem. Sci.*, 2026, **17**, 2506

Electrosynthesis of 2,5-furandicarboxylic acid from 5-hydroxymethylfurfural: mechanisms, advanced catalysts, and reaction microenvironments

Jiacheng Zhang,†[ab] Siping Wang,†[ab] Jiaqing Liu,[ab] Jiayi Chen,[ab] Guigang Zhang,[ab] Yidong Hou,[ab] Meifang Zheng,*[ab] Sibo Wang*[ab] and Xue Feng Lu*[ab]

As the sole renewable source of organic carbon, biomass is indispensable to the green transition, offering both abundance and carbon neutrality. The biomass-derived platform molecule, 5-hydroxymethylfurfural (HMF), can be valorized into various high-value chemicals *via* oxidation. Most notably, 2,5-furandicarboxylic acid (FDCA) has emerged as a crucial sustainable alternative to fossil-based terephthalic acid for polyester production. This review provides a comprehensive analysis of the electrocatalytic oxidation of HMF to FDCA. We begin by dissecting the reaction pathways and mechanisms to clarify key kinetic steps and current bottlenecks. To establish benchmarks for the field, we summarize standard evaluation metrics that enable rigorous comparison among disparate studies. The review then systematically categorizes diverse catalyst systems and engineering strategies, with a specific focus on how reaction parameters (pH, electrolyte composition, and applied potential) dictate product selectivity. Concluding with a forward-looking perspective, we propose future directions to accelerate the development of efficient, controllable, and low-cost technologies for FDCA production.

Received 11th December 2025
Accepted 12th January 2026

DOI: 10.1039/d5sc09723a

rsc.li/chemical-science

1 Introduction

The imperative to mitigate fossil fuel dependence and environmental degradation has catalyzed the search for sustainable chemical feedstocks.[1,2] As the sole renewable source of organic carbon, biomass offers a pivotal pathway toward carbon neutrality.[3–6] Among biomass-derived platform molecules, 5-hydroxymethylfurfural (HMF) is particularly versatile, possessing a furan-rich architecture amenable to upgrading into high-value derivatives.[7–9] Notably, 2,5-furandicarboxylic acid (FDCA) has emerged as a paramount bio-based alternative to petroleum-derived terephthalic acid, underpinning the production of sustainable polyesters.[10,11] While traditional thermocatalytic and biocatalytic routes are often hampered by harsh conditions or kinetic limitations, electrocatalytic oxidation presents a compelling "green" alternative.[12,13] This approach leverages mild conditions and renewable electricity to

[a]*State Key Laboratory of Chemistry for NBC Hazards Protection, College of Chemistry, Fuzhou University, Fuzhou 350116, China. E-mail: mfzheng@fzu.edu.cn; sibowang@fzu.edu.cn; luxf@fzu.edu.cn*

[b]*State Key Laboratory of Photocatalysis on Energy and Environment, College of Chemistry, Fuzhou University, Fuzhou 350116, China*

† These authors contributed equally to this work.

Jiacheng Zhang

Jiacheng Zhang received his BSc degree in 2024 from Fuzhou University. He is currently a PhD student under the supervision of Prof Xue Feng Lu at Fuzhou University. His research interests lie in the design and synthesis of highly efficient electrocatalysts, with a specific focus on elucidating the mechanisms underlying water splitting and small organic molecule electro-oxidation.

Siping Wang

Siping Wang received her BSc degree in 2024 from Hengyang Normal University. She is currently an MSc student under the supervision of Prof Xue Feng Lu at Fuzhou University. Her research focuses on the design and synthesis of nickel-based catalysts and the investigation of their performance and mechanisms in the electrocatalytic oxidation of 5-hydroxymethylfurfural.

drive valorization, yet developing systems that simultaneously achieve high current density and rigorous selectivity for FDCA remains a formidable challenge.[13,14]

The complexity of the electrocatalytic HMF oxidation reaction (HMFOR) arises from its multi-electron, proton-coupled nature, which spawns a branched reaction network yielding intermediates, such as 2,5-diformylfuran (DFF), 5-hydroxymethyl-2-furancarboxylic acid (HMFCA), and 5-formyl-2-furancarboxylic acid (FFCA). Consequently, suppressing byproducts requires precise modulation of the reaction kinetics. Extensive efforts have focused on tailoring catalyst intrinsic activity through doping, defect engineering, and heterostructure design across diverse material classes, from noble metals to transition metal-based electrocatalysts, and even metal-free electrocatalysts.[15–21] However, catalyst design cannot be viewed in isolation. The local reaction microenvironment, dictated by electrolyte pH, composition, and applied potential, exerts a profound, often governing influence on adsorption energies and reaction pathways.[22] Thus, a holistic strategy that synergizes rational electrode design with electrolyte engineering is indispensable for achieving efficient and selective FDCA electrosynthesis.[23]

This review distinguishes itself by bridging the gap between material synthesis and reaction condition optimization in the HMFOR. Moving beyond a mere catalog of catalyst performance, we aim to elucidate the interplay between surface chemistry and the reaction environment. As shown in Fig. 1, we begin by dissecting reaction mechanisms and kinetic bottlenecks to establish a fundamental framework. Subsequently, we define standardized evaluation metrics to facilitate rigorous benchmarking across the field. The core of this review systematically analyzes how catalyst architecture and operating parameters (pH and potential) jointly determine product selectivity. Finally, we provide a forward-looking perspective on emerging trends, offering a roadmap for the development of

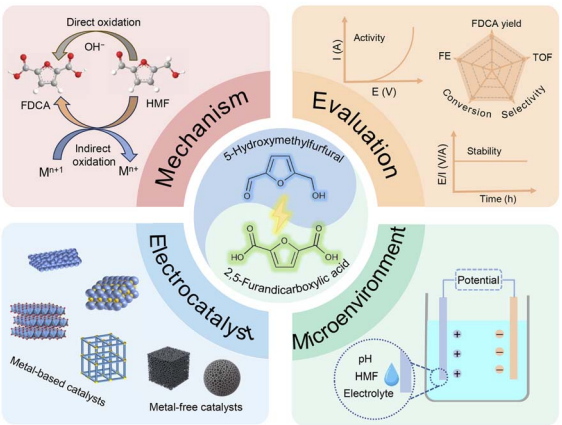

Fig. 1 Schematic diagram of the mechanism, catalyst design, microenvironmental regulation, and performance evaluation in the electrosynthesis oxidation of HMF to FDCA.

Meifang Zheng

Dr Meifang Zheng is a Professor at the State Key Laboratory of Photocatalysis on Energy and Environment, Fuzhou University. She obtained her PhD degree from South China University of Technology in 2016 and continued her postdoctoral training at Fuzhou University. In 2019, she joined Fuzhou University. Her research interests focus on functional semiconductors for selective organic transformations.

Sibo Wang

Dr Sibo Wang is a Professor at the State Key Laboratory of Photocatalysis on Energy and Environment, Fuzhou University. He obtained his PhD degree from Fuzhou University in 2016 and then went to Nanyang Technological University for postdoctoral research. In 2020, he was recruited at Fuzhou University as a Professor through the Global Recruitment Program of China. His main research interests are photocatalytic CO_2 reduction, CH_4 conversion, and water splitting. He has published over 140 peer reviewed papers with more than 18000 citations and an H-index of 62, and was selected as a Highly Cited Researcher by Clarivate from 2020 to 2025.

Xue Feng Lu

Dr Xue Feng Lu is currently a full professor at the State Key Laboratory of Photocatalysis on Energy and Environment, Fuzhou University, China. He obtained his PhD degree from Sun Yat-sen University in June 2017. He carried out postdoctoral research at Nanyang Technological University, Singapore, and The Hong Kong Polytechnic University from August 2017 to July 2022. His research interests focus on the design and synthesis of advanced functional materials towards electrochemical energy storage and conversion. He has published over 90 peer-reviewed papers with more than 17000 citations and an H index of 57, and was selected as a Highly Cited Researcher by Clarivate from 2021 to 2025.

controllable, cost-effective, and scalable FDCA production technologies.

2 Reaction pathway and mechanism of the HMFOR

2.1 Reaction pathway

The HMFOR in alkaline media is a 6-electron transfer process yielding FDCA.[24] This transformation proceeds *via* intricate intermediate steps regulated by catalyst surface kinetics and reaction conditions. As illustrated in Fig. 2, the reaction bifurcates into two primary routes.[25,26] Path 1 involves the preferential oxidation of the hydroxymethyl group (–CH_2OH) to generate DFF, which is subsequently oxidized to FFCA and then FDCA. Path 2 proceeds *via* the preferential oxidation of the aldehyde group (–CHO) to form HMFCA, followed by the oxidation of the remaining hydroxyl group to FFCA and finally FDCA. The reaction selectivity is highly sensitive to operating parameters; for instance, mild alkalinity (pH < 13) typically favors the DFF pathway, whereas strong alkalinity (pH > 13) promotes the HMFCA pathway.[27,28]

Currently, the HMFOR pathway analysis relies heavily on offline high-performance liquid chromatography (HPLC).[29] However, this method is limited by long detection cycles and an inability to capture real-time dynamics. In contrast, *in situ* characterization techniques offer superior advantages for mechanistic studies. For instance, *in situ* sum frequency generation (SFG) and infrared (IR) spectroscopy have been employed to monitor HMFOR, enabling the real-time tracking of key intermediate evolution.[30,31] Looking forward, the integration of *in situ* techniques with higher spatiotemporal resolution will be essential to provide direct, precise evidence for a comprehensive understanding of the reaction mechanism.

2.2 Reaction mechanism

The HMFOR mechanism is generally categorized into direct and indirect oxidation. The direct pathway, often termed the OH* mechanism, is characterized by the co-adsorption of HMF and OH^- on the catalyst surface, where oxidation proceeds *via* direct electron transfer without altering the catalyst's oxidation state.[32,33] In this process, the adsorption energy of HMF plays a crucial role in the reaction activity.[34] Insufficient adsorption leads to low activation and cleavage efficiency of C–H and O–H bonds, while excessive adsorption inhibits the adsorption of surface OH^- species. In Pathway 1, surface-adsorbed OH^- generates OH* active species that activate the –CH_2OH group of HMF, cleaving O–H and C–H bonds to form DFF. Subsequently, the –CHO group in DFF undergoes nucleophilic attack by water to form a gem-diol intermediate, which is further oxidized *via* OH*-assisted dehydrogenation to FFCA and finally FDCA. Conversely, Pathway 2 initiates with water attacking the –CHO group of HMF. The resulting diol intermediate is converted to HMFCA *via* OH*-assisted bond cleavage. The –CH_2OH group of HMFCA is then activated by OH*, leading to FFCA, which transforms into FDCA through analogous addition–deprotonation steps.

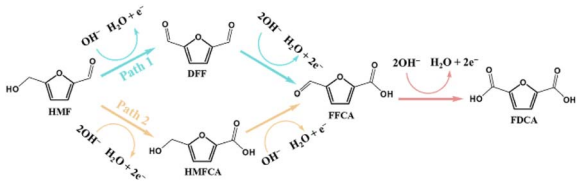

Fig. 2 Reaction pathway for the electrocatalytic conversion of HMF to FDCA.

Complementary to direct oxidation, the HMFOR may also proceed *via* an indirect "electrochemical–chemical (E–C)" mechanism.[35] This pathway is characterized by the initial electrochemical generation of strongly oxidizing species, which subsequently oxidize HMF *via* chemical steps rather than direct electron transfer.[36–38] Indirect oxidation is generally categorized into heterogeneous and homogeneous modes.[8] In heterogeneous systems, applied potentials drive the transformation of low-valent metal centers into high-valent active species (*e.g.*, Ni^{3+} and Co^{3+}) with potent oxidative capabilities. The formation of these species is critically dependent on the potential and surface OH^- concentration. Consequently, facilitating the onset of high-valent states is a key strategy for enhancing activity. For instance, Liu *et al.* demonstrated that incorporating Pd nanoparticles into NiFe layered double hydroxide (NiFe–LDH) creates abundant Ni vacancies, which lowers the oxidation potential of Ni sites and significantly boosts catalytic performance.[39] Beyond their formation, the kinetics of the subsequent reduction of high-valent species back to lower oxidation states (*e.g.*, the reduction of Ni^{3+} to Ni^{2+}) constitute a critical determinant of the attainable current density, as a rapid redox cycle enables the sustained generation of reactive oxidizing centers during operation.[40] In homogeneous systems, soluble redox mediators such as 2,2,6,6-tetramethylpiperidinyloxyl (TEMPO) and 4-acetamido-TEMPO (ACT) are employed.[41] Here, the mediator is electrochemically oxidized to its active form (*e.g.*, $TEMPO^+$), which then chemically oxidizes HMF before regenerating the resting state. Notably, unlike heterogeneous pathways, this cycle typically proceeds independently of surface OH^-.[42]

Crucially, direct and indirect mechanisms often coexist, with their relative dominance dictated by the catalyst identity and reaction conditions. Disentangling these competitive pathways requires a combination of *in situ* characterization to identify key oxidizing species and Density Functional Theory (DFT) calculations to probe their specific interactions with HMF molecules.[43,44]

3 Evaluation criteria and methods

In HMFOR research, the rigorous evaluation of catalyst performance is fundamental for both screening high-efficiency materials and elucidating reaction mechanisms. Standard assessment protocols encompass three critical dimensions: catalytic activity, conversion efficiency, and stability. The following section outlines the significance of these metrics, along with the respective testing methodologies and calculation procedures employed to quantify them.

3.1 Onset potential

The onset potential defines the voltage threshold at which the anodic current first deviates significantly from the baseline, marking the initiation of the electrochemical reaction. In HMFOR studies, this parameter is typically determined *via* linear sweep voltammetry (LSV). A lower onset potential indicates that the catalyst can drive the reaction with a lower energy input, reflecting superior intrinsic activity.[45] Practically, this metric is directly correlated with the system's energy consumption, making it a critical indicator of energy efficiency.[46] Crucially, to ensure valid comparability across different studies, onset potentials must be measured under strictly standardized conditions, controlling for HMF concentration, electrolyte composition, pH, scan rate, and electrode geometric area.

3.2 Tafel slope

The Tafel slope is a fundamental kinetic parameter that quantifies the dependence of the current density on overpotential.[47] It is typically derived from the linear region of an LSV or steady-state polarization curve using the Tafel equation:

$$\eta = a + b \log j$$

where η represents the overpotential, j is the current density, and b denotes the Tafel slope (mV dec^{-1}). This parameter reflects the sensitivity of the reaction rate to potential changes. A smaller slope indicates faster kinetics, implying that a smaller increase in overpotential is required to significantly boost the current.[46] Experimentally, the slope must be calculated from the steady-state region where mass transport limitations are negligible. The magnitude of the Tafel slope is governed by the catalyst's surface properties and charge transfer efficiency, and it provides insight into the rate-determining step (RDS) of the mechanism, such as the first electron transfer or chemical adsorption steps.[48] Consequently, the Tafel slope is often analyzed in conjunction with the onset potential to provide a comprehensive evaluation of intrinsic catalytic activity.

3.3 Turnover frequency (TOF)

TOF is the definitive metric for evaluating intrinsic catalytic activity, defined as the number of catalytic turnovers per active site per unit time.[49] By normalizing activity to the number of active centers, TOF decouples intrinsic efficiency from extrinsic factors such as surface area and conductivity.[50] A higher TOF signifies superior site-specific kinetics and atomic utilization, which is essential for the design of high-performance, low-loading catalysts. TOF is calculated using the following equation:

$$\mathrm{TOF}\ \left(\mathrm{s}^{-1}\right) = \frac{jA}{znF}$$

where j represents the current density, A is the geometric electrode area, z is the electron transfer number (*e.g.*, 6 for HMF → FDCA), F is the Faraday constant (96 485 C mol^{-1}), and n denotes the molar quantity of active sites. Since directly measuring n is difficult, it is often estimated electrochemically, for instance, by integrating the redox peak area (*e.g.*, Ni^{2+}/Ni^{3+}) in cyclic voltammetry (CV). For reliability, TOF measurements should be conducted at low HMF conversion levels (<10%) to avoid interference from mass transport constraints or product accumulation.

3.4 Electrochemically active surface area (ECSA)

The ECSA is a critical parameter quantifying the electrode surface accessible for electrochemical reactions, serving as a direct proxy for the effective catalytic interface. Unlike the geometric area, the ECSA provides a more accurate representation of the number of active sites, making it particularly valuable for evaluating complex, porous, or nanostructured materials.[51] Generally, a larger ECSA implies a greater abundance of exposed active sites per unit mass or area, which correlates with enhanced electrocatalytic performance. The most prevalent method for determining the ECSA relies on measuring the electrochemical double-layer capacitance (C_{dl}) *via* CV curves.[52] Measurements are conducted within a non-faradaic potential window. By recording CV curves at different scan rates, the capacitive current density is plotted as a function of scan rate, and a linear relationship is obtained. The slope of this linear fit corresponds to C_{dl}. Consequently, the ECSA is estimated by normalizing this value against the specific capacitance of a standard flat surface (C_s) using the following formula:

$$\mathrm{ECSA} = \frac{C_{dl}}{C_s}$$

3.5 Electrochemical Impedance Spectroscopy (EIS)

EIS is widely employed as an auxiliary electrochemical method to elucidate interfacial electron-transfer dynamics and transport phenomena in electrocatalytic systems.[53] Through the application of a small-amplitude alternating potential over a frequency range spanning from high to low values, EIS enables the quantitative analysis of key interfacial parameters, including charge-transfer resistance (R_{ct}), interfacial capacitance, and diffusion-controlled processes at the electrode–electrolyte boundary.[54] In the HMFOR, EIS is typically performed at catalytically relevant potentials, and the resulting spectra are analyzed using equivalent circuit models to extract the R_{ct}.[55] A lower R_{ct} generally indicates faster interfacial electron transfer and more efficient charge transport. Accordingly, EIS offers important insights into the relationship between catalytic activity and interfacial properties, and its combination with activity and selectivity metrics improves the reliability and comparability of electrocatalyst evaluation.

3.6 Conversion

Monitoring the depletion of HMF is essential for tracking the progress of electrocatalytic oxidation. HMF conversion quantifies the fraction of the initial reactant consumed, thereby serving as a primary metric for the catalyst's overall oxidative efficiency. This value is typically determined *via* HPLC by analyzing the change in HMF concentration before and after electrolysis.[56] The conversion is calculated using the following equation:

$$\text{Conversion}\ (\%) = \frac{n_{\text{HMF initial}} - n_{\text{HMF instant}}}{n_{\text{HMF initial}}} \times 100\%$$

where $n_{\text{HMF initial}}$ and $n_{\text{HMF instant}}$ represent the amount of HMF at the beginning of the reaction and at a specific time point, respectively.

3.7 Faraday efficiency (FE)

FE is a critical metric for evaluating electron utilization in electrocatalytic reactions, representing the percentage of the total charge passed that is utilized to generate the desired product.[57] In the HMFOR, FE reflects the catalyst's selectivity and its capacity to direct electron flux toward the synthesis of target products rather than side reactions. Quantitatively, it is determined by comparing the theoretical charge required for the measured product yield against the total experimental charge passed through the electrode. The calculation is performed using the following equation:

$$\text{FE}\ (\%) = \frac{z \times n_{\text{product}} \times F}{Q} \times 100\%$$

where z is the number of electrons transferred per molecule of product formed, n_{product} is the molar amount of the product determined by quantitative analysis (*e.g.*, HPLC), F is the Faraday constant, and Q is the total charge passed during electrolysis, obtained by integrating the current–time (I–t) curve.

3.8 Yield

Yield quantifies the fraction of the initial HMF load that is successfully converted into the target product, making it a definitive parameter for evaluating catalyst effectiveness. Unlike conversion, which tracks only substrate consumption, yield accounts for the actual generation of the desired species. Consequently, it offers a more accurate reflection of the catalyst's capacity to selectively drive the reaction toward the target pathway. In practice, the product yield is typically determined by quantitative analysis of liquid-phase products using HPLC. The calculation is performed as follows:

$$\text{Yield}\ (\%) = \frac{n_{\text{product}}}{n_{\text{HMF initial}}} \times 100\%$$

3.9 Selectivity

Selectivity characterizes the propensity of a catalyst to generate a specific target product (*e.g.*, FDCA, HMFCA, or DFF) amidst a complex network of competing oxidation pathways. This parameter reflects the catalyst's capacity to direct the reaction mechanism, making it a critical indicator for evaluating performance, controlling product distribution, and suppressing side reactions. Selectivity is typically calculated as the ratio of the molar quantity of the specific product formed to the amount of HMF consumed, as expressed below:

$$\text{Selectivity}\ (\%) = \frac{n_{\text{product}}}{n_{\text{HMF consumed}}} \times 100\%$$

3.10 Stability

High stability is a prerequisite for industrial viability, ensuring that a catalyst maintains both activity and structural integrity during prolonged operation.[58] Stability is typically assessed *via* chronoamperometry (CA) or chronopotentiometry (CP), which monitors the evolution of current density or potential over time. However, a critical challenge in these measurements is the continuous consumption of HMF; as the substrate concentration decreases, the current may drop, creating a false impression of catalyst deactivation. To decouple substrate depletion from intrinsic catalyst degradation, HMF must be regularly replenished, or the catalyst should be subjected to multi-cycle recycling tests.[59] Furthermore, post-reaction characterization is essential. Techniques such as scanning electron microscopy (SEM) and X-ray photoelectron spectroscopy (XPS) should be employed to compare the catalyst before and after testing, providing insight into structural evolution and phase stability. Finally, monitoring the retention of product yield and selectivity over time is crucial for a comprehensive evaluation of the catalyst's practical durability and application potential.

4 Electrocatalysts

Since the catalyst serves as the active site for the reaction, the rational design and development of electrode materials are of paramount importance for the HMFOR. Recent years have witnessed significant advancements in this field, with a diverse array of materials developed to enhance performance. These catalysts encompass a broad spectrum, ranging from metals and alloys to various compounds, including oxides, hydroxides, sulfides, and phosphides, as well as metal-free systems.[60] Notably, transition metal-based catalysts (particularly Ni, Co, and Fe) have garnered the most interest. This preference stems from their versatile redox chemistry, superior electronic conductivity, and the high tunability of their surface-active sites. The following sections provide a systematic review of recent breakthroughs across these various categories.

4.1 Metals/alloys

Pure metal electrocatalysts are susceptible to corrosion in acidic and alkaline electrolytes. Therefore, introducing stable structures (such as carbon materials) to enhance their durability in harsh electrolytes has become a common strategy. Lu *et al.* prepared an efficient HMFOR catalyst (Ni/CP) by electrodepositing Ni nanosheet (NS) forests onto carbon paper.[61] As shown in Fig. 3a, the catalyst exhibited excellent stability and a high FDCA selectivity of 99.4% at 1.36 V *vs.* RHE (reversible hydrogen electrode). Unless otherwise specified, all potential values reported below are referred to the RHE. In addition, Li *et al.* constructed a Ni@C composite structure by employing a citric acid-assisted sol–gel method followed by high-temperature carbonization, in which metallic nickel was uniformly encapsulated within a carbon layer.[62] The carbon coating facilitated the *in situ* redistribution of Ni nanoparticles into smaller-sized $NiOOH_x$ ($x < 1$), thereby increasing the electrochemically active surface area and promoting the formation

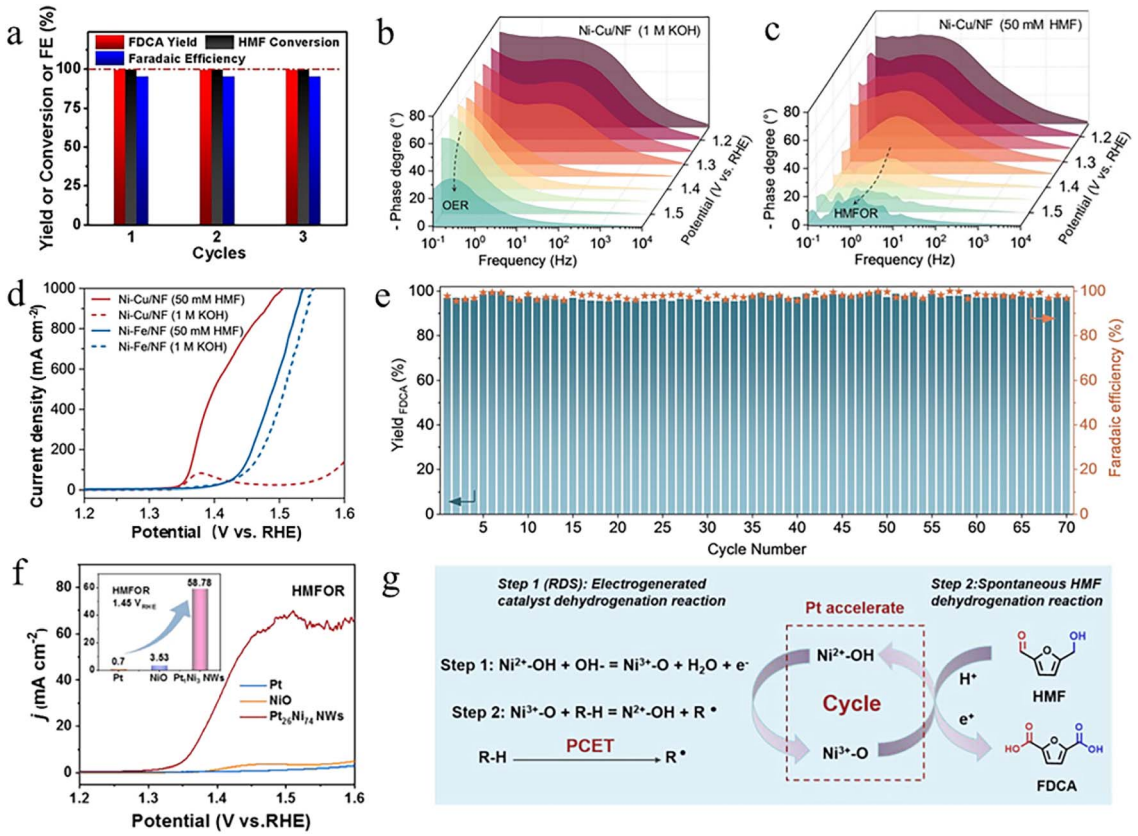

Fig. 3 (a) Conversion of HMF, yields of FDCA and H_2 FE for consecutive applications of the Ni(NS)/CP electrode (1.36 V).[61] Copyright 2021, Wiley-VCH GmbH. (b and c) *Operando* EIS spectra of NiCu/NF at different potentials in the absence/presence of 50 mM HMF. (d) LSV curves of NiCu/NF and NiFe/NF with and without 50 mM HMF in 1 M KOH solution with 100% *iR* compensation. (e) Stability evaluation, yield, and FE of FDCA for NiCu/NF with 50 mM HMF over 70 successive cycles at 1.45 V, 60 min for each cycle.[15] Copyright 2021, Wiley-VCH GmbH. (f) LSV curves of $Pt_{26}Ni_{74}$ NWs, bulk Pt, and NiO in 1 M KOH without/with HMF. (g) Schematic diagram of the HMFOR mechanism, including the electrocatalyst function and nonelectrochemical step on $Pt_{26}Ni_{74}$ NWs.[64] Copyright 2022, American Chemical Society.

of active Ni sites. Further experimental results and DFT calculations revealed that $NiOOH_x$ exhibited a more favorable thermodynamic driving force for the oxidation of the formyl and hydroxymethyl groups in HMF, thus significantly enhancing the overall performance of the HMFOR process. Compared to pure metals, alloy systems with more complex structures and compositions can significantly enhance catalytic activity by leveraging synergistic effects.[63] For example, to suppress this competing oxygen evolution reaction (OER) process in the HMFOR, Chen *et al.* reported a bimetallic NiCu catalyst supported on Ni foam (Ni–Cu/NF).[15] *Operando* EIS analysis reveals distinct kinetic behaviors between the OER and HMFOR on Ni–Cu/NF. Under OER conditions, the emergence of low-frequency signals above 1.55 V indicates sluggish O_2 evolution kinetics (Fig. 3b). In contrast, the HMFOR exhibits characteristic mid-frequency responses concurrent with Ni^{3+} formation, suggesting that highly oxidized Ni species preferentially facilitate the HMFOR rather than the OER (Fig. 3c). Fig. 3d shows that Ni–Cu/NF exhibits excellent HMFOR activity and poor OER performance, indicating that the introduction of Cu effectively suppresses the competing OER. Fig. 3e shows the excellent performance and stability of Ni–Cu/NF toward the HMFOR. Throughout 70 consecutive electrolysis cycles, both the FE and the yield of FDCA remain above 95%. Moreover, Wu *et al.* synthesized a PtNi alloy catalyst, which exhibited significantly enhanced performance compared to pure Pt and NiO (Fig. 3f).[64] The enhanced performance is attributed to the introduction of Pt, which accelerates the oxidation of Ni^{2+}–OH to Ni^{3+}–O. Additionally, the PtNi bimetallic catalyst facilitates the formation of stable active oxygen species (Pt–O–Ni), effectively regulating the adsorption behavior of HMF and OH^-, thereby improving the HMFOR activity (Fig. 3g).

4.2 Metal oxides

Metal oxides have attracted widespread attention in the field of electrocatalysis due to their tunable oxidation states, diverse crystal structures, high catalytic activity, and excellent stability.[65,66] In recent years, researchers have developed a variety of highly efficient metal oxide catalysts and significantly improved their electrocatalytic performance by controlling their electronic structure and surface activity through defect engineering, doping, and interface engineering. Notably, cobalt-based spinel oxides have been widely used in the study of the HMFOR due to their high structural tunability and

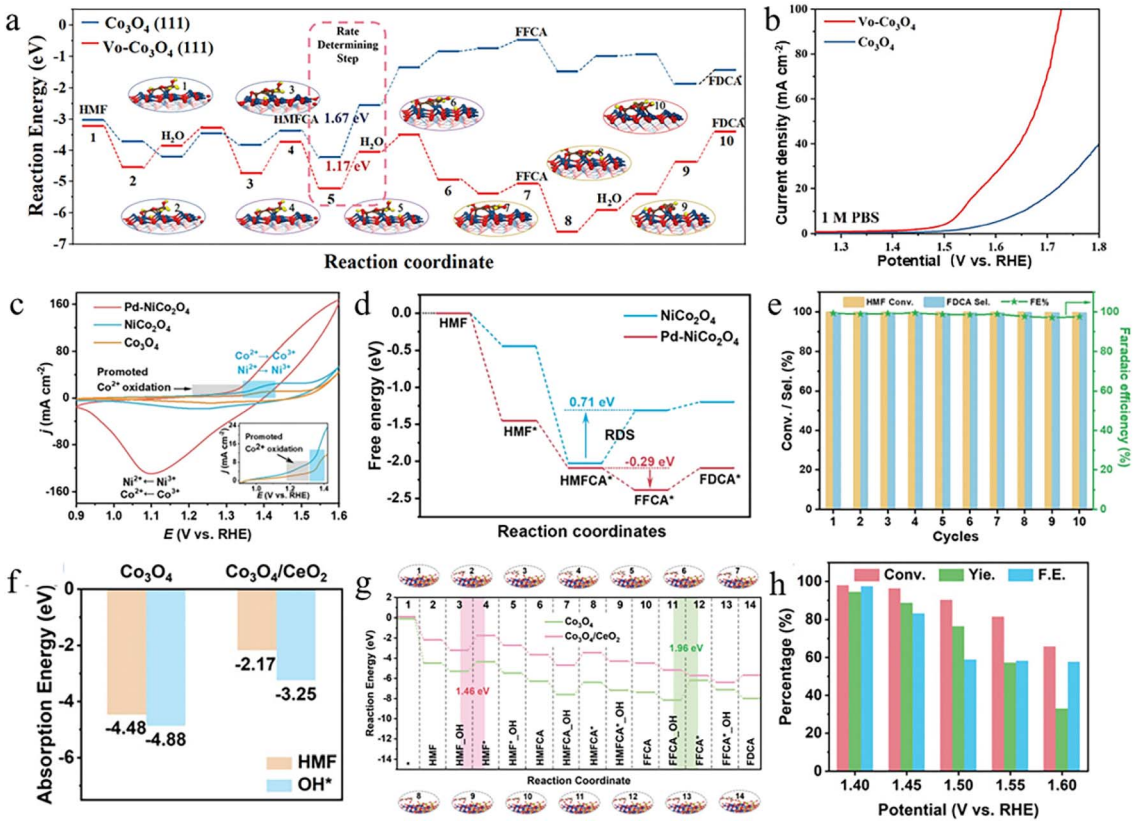

Fig. 4 (a) Free energies of the HMFOR step on Ov–Co_3O_4 and Co_3O_4. (b) The LSV curves of Ov–Co_3O_4 and Co_3O_4 in 1 M PBS with 50×10^{-3} M HMF.[22] Copyright 2021, Wiley-VCH GmbH. (c) CV curves of Co_3O_4, $NiCo_2O_4$, and Pd–$NiCo_2O_4$ in 1 M KOH. (d) Corresponding free energy diagram on $NiCo_2O_4$ and Pd–$NiCo_2O_4$ http://creativecommons.org/licenses/by/4.0/. (e) FE, selectivity of FDCA, and the conversion of HMF obtained by the Pd–$NiCo_2O_4$ over ten consecutive cycles of the HMFOR.[68] Copyright 2024, Springer Nature. Distributed under the terms of the Creative Commons CC BY license (http://creativecommons.org/licenses/by/4.0/). (f) HMF and OH* adsorption free energy of Co_3O_4 and Co_3O_4/CeO_2. (g) Free energies of the HMFOR step on Co_3O_4 and Co_3O_4/CeO_2, and adsorption configurations of HMFOR intermediates on Co_3O_4/CeO_2. (h) The HMF conversion, FDCA yield, and FE at different potentials for NF@Co_3O_4/CeO_2.[69] Copyright 2023, Wiley-VCH GmbH.

abundant active sites. Lu *et al.* synthesized Co_3O_4 nanosheets *via* electrodeposition and applied them to the HMFOR, demonstrating an FDCA yield of 86.7% at 1.44 V.[22] Subsequently, oxygen vacancies (Ov) were introduced *via* Ar plasma treatment to modulate the electronic structure and enhance the intrinsic catalytic activity of Co_3O_4. To elucidate the role of Ov in the HMFOR process, DFT calculations were performed by comparing the reaction free energy profiles on pristine Co_3O_4 and oxygen-deficient Co_3O_4 surfaces (Fig. 4a). The results show that the introduction of Ov significantly lowers the Gibbs free energy barrier of the HMFCA dehydrogenation step from 1.67 eV to 1.17 eV, thereby promoting the overall HMFOR kinetics. Combined experimental and theoretical analyses further reveal that nucleophilic OH^- preferentially occupies the Ov sites in Ov–Co_3O_4, forming lattice OH species that directly participate in the dehydrogenation and coupling processes of HMF intermediates. Consequently, Ov–Co_3O_4 exhibits an enhanced catalytic performance with an FDCA yield of up to 91.9% (Fig. 4b). In addition to modifying the electronic structure of Co_3O_4 itself through defect engineering, Lu *et al.* also introduced a single Ir atom into Co_3O_4 to construct Ir–Co_3O_4.[67] This structure enhances its adsorption capacity for C=C bonds in HMF, thereby significantly improving catalytic performance, with the FDCA yield reaching as high as 98%. To further improve catalytic performance and FDCA selectivity, Jiang *et al.* synthesized a Pd–$NiCo_2O_4$ catalyst by doping Ni into the Co_3O_4 lattice to form $NiCo_2O_4$ and subsequently integrating Pd clusters on the $NiCo_2O_4$ surface.[68] The Ni doping promoted the generation of active Co^{3+}–O species and the oxidation of OH^- to electron-deficient OH*, thereby facilitating the direct oxidation process (Fig. 4c). Meanwhile, the introduction of Pd optimized the adsorption behavior of HMF and OH^- species. These synergistic effects enhanced the electron/charge transfer activity in the HMFOR and promoted the key deprotonation step of HMFCA (Fig. 4d). Pd–$NiCo_2O_4$ exhibits excellent FDCA selectivity (99.2%) and FE (99.6%) at 1.5 V (Fig. 4e). Besides metal doping and noble metal loading, constructing heterojunctions to further enhance catalytic activity and product selectivity is also an effective regulatory strategy. For example, Zhao *et al.* successfully synthesized a NF@Co_3O_4/CeO_2 electrocatalyst with Co_3O_4 nanowires as the "core" and CeO_2 nanoparticle layer as the "shell".[69] The CeO_2 modification on the Co_3O_4 surface constructs Co_3O_4/CeO_2 heterointerfaces whose interfacial active centers effectively regulate the adsorption

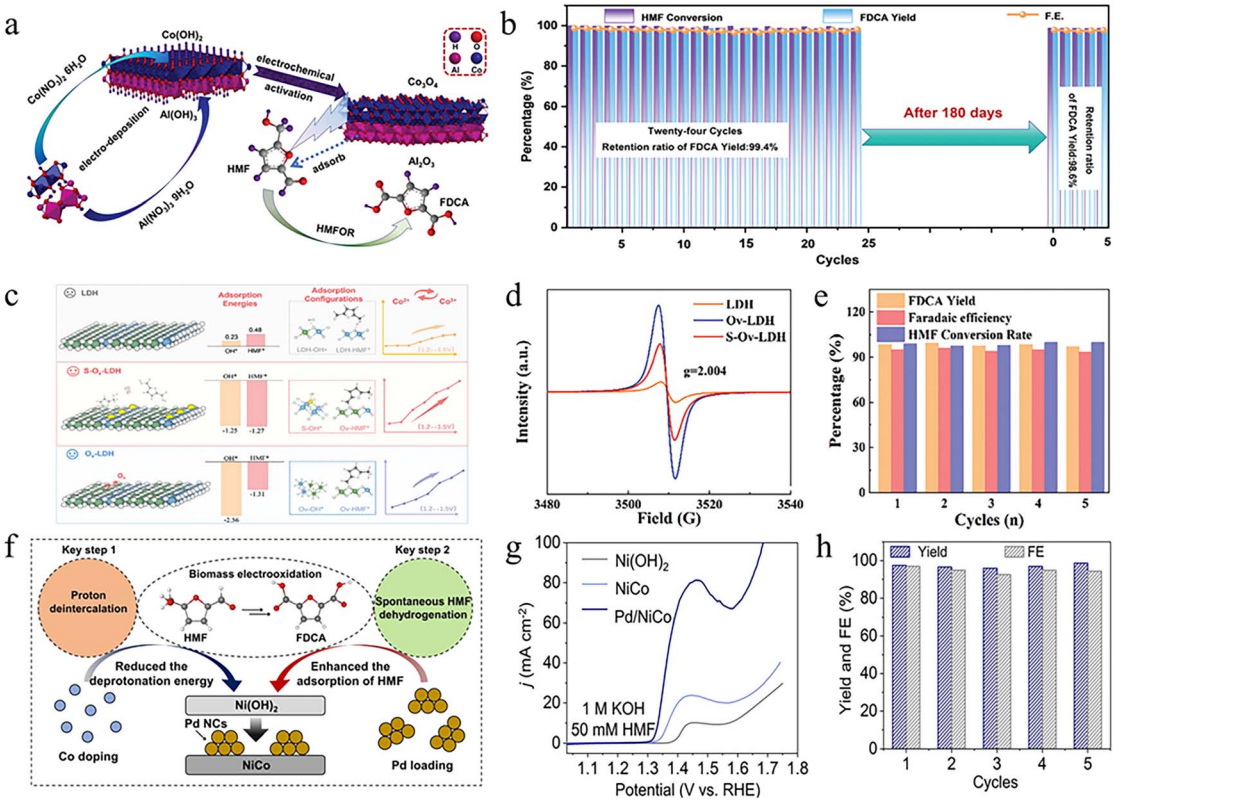

Fig. 5 (a) Schematic diagram of $Al(OH)_3/Co(OH)_2$ synthesis and electrochemical system of the HMFOR. (b) HMF conversion, FDCA yield, and FE over-activated $Al(OH)_3/Co(OH)_2$ during twenty-four successive HMF oxidations (1.5 V, 10 mM HMF, 1 M KOH).[74] Copyright 2024, Wiley-VCH GmbH. (c) The diagram of the catalytic enhancement mechanism of S–Ov–LDH. (d) EPR spectrum of the LDH, Ov–LDH, and S–Ov–LDH samples. (e) FE and FDCA yield of S–Ov–LDH under five successive electrolysis cycles.[18] Copyright 2024, Wiley-VCH GmbH. Distributed under the terms of the Creative Commons CC BY license (http://creativecommons.org/licenses/by/4.0/). (f) The Co-doping and Pd loading strategy for promoting two key steps of proton deintercalation and spontaneous HMF dehydrogenation by using Pd/NiCo. (g) LSV curves of $Ni(OH)_2$, NiCo, and Pd/NiCo at 1 M KOH and 50 mM HMF solution at 5 mV s^{-1}. (h) The FDCA yield and FE on Pd/NiCo.[75] Copyright 2023, Wiley-VCH GmbH.

behavior of key intermediates and facilitate electron transfer. As shown in Fig. 4f, the heterointerface moderates the adsorption strengths of HMF and OH* compared with pristine Co_3O_4, which is beneficial for both reactant activation and subsequent product desorption. In addition, the reaction free energy profiles (Fig. 4g) show that the rate-determining step for Co_3O_4 shifts from FFCA → FDCA, with a maximum energy change of 1.96 eV, to HMF → HMFCA in the Co_3O_4/CeO_2 heterostructure, where the energy barrier is reduced to 1.46 eV, thereby significantly improving the overall HMFOR kinetics. Consequently, the catalyst exhibited 94.5% FDCA yield and 97.5% FE at 1.40 V (Fig. 4h). Furthermore, Zhou *et al.* constructed a CuO–PdO heterojunction. The intrinsically low OER activity of CuO effectively suppresses competitive reactions.[70] The presence of PdO significantly enhances the adsorption and conversion of HMF and OH^- species, particularly facilitating dehydrogenation and electron transfer during the conversion of FFCA to FDCA, improving the HMFOR performance.

4.3 Metal hydroxides

As early as 1991, studies had reported the use of metal-based hydroxides to catalyze the HMFOR.[71] As a class of catalysts with great application potential, metal-based hydroxides have attracted increasing attention in recent years.[72] Early studies explored the use of single metal hydroxides for the HMFOR. However, their low conductivity, limited active site exposure, and unbalanced adsorption behavior often resulted in unsatisfactory catalytic activity. To address these intrinsic limitations, it has been recognized that the orbital-level electronic structure regulation of transition-metal active sites can improve substrate adsorption and reaction kinetics. Chen *et al.* reported a Mn-modified $Ni(OH)_2$ catalyst supported on a porous metallic skeleton, in which gradient d–d orbital occupancy was engineered *via* the incorporation of $Mn^{3+/4+}$ species with low 3d electron filling and high spin states.[73] The resulting d–d orbital hybridization between Mn and Ni redistributes 3d electrons, increases unoccupied antibonding states, and strengthens d–p hybridization, thereby optimizing HMF adsorption and facilitating electron transfer during the HMFOR. Consequently, the Mn–$Ni(OH)_2$ catalyst delivered a current density exceeding 1.2 A cm^{-2} at 1.42 V, while maintaining excellent FDCA yield and FE over multiple cycles. Beyond intrinsic electronic structure regulation, researchers further began developing composite hydroxides that combine complementary components to enhance both activity and selectivity. For instance, Dai *et al.* synthesized an $Al(OH)_3/Co(OH)_2$ catalyst by electrodeposition

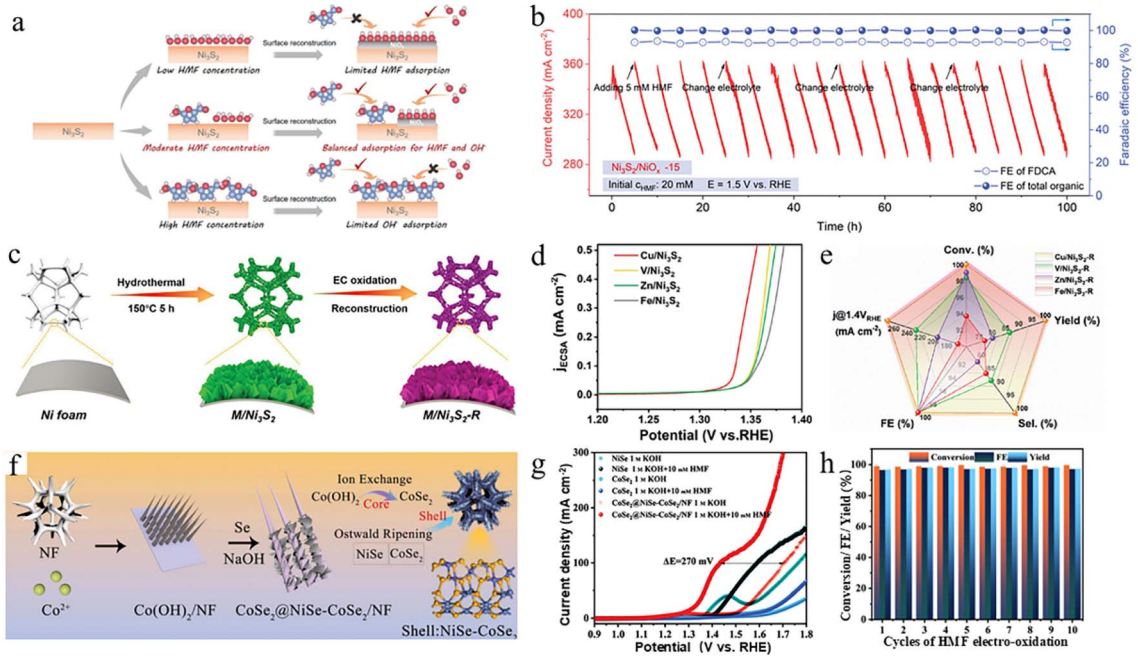

Fig. 6 (a) Schematic illustration of the *in situ* controlled surface reconstruction of Ni_3S_2. The degree of surface reconstruction can be controlled by adjusting HMF coverage of the Ni_3S_2 surface. The blue, red, and white balls represent carbon, oxygen, and hydrogen atoms, respectively. (b) Current density of Ni_3S_2/NiO_x-15 and FE of the products during chronoamperometry measurements for over 100 h.[82] Copyright 2023, Wiley-VCH GmbH. (c) Schematic illustration for the synthesis of M/Ni_3S_2–R electrocatalysts (M = Fe, Zn, V, and Cu). (d) ECSA-normalized LSV curves for the HMFOR. (e) Performance comparison of M/Ni_3S_2–R.[83] Copyright 2023, Wiley-VCH GmbH. (f) Schematic of the preparation method of $CoSe_2$@NiSe–$CoSe_2$/NF. (g) LSV curves of NiSe, $CoSe_2$, and $CoSe_2$@NiSe–$CoSe_2$/NF in 1 M KOH with and without 10 mM HMF. (h) Yield, HMF conversion rate, and FE of the $CoSe_2$@NiSe–$CoSe_2$/NF during ten electrolysis cycles.[21] Copyright 2025, Wiley-VCH GmbH.

followed by electrochemical activation.[74] In this system, Co^{3+} serves as the primary active site for the electrocatalytic HMFOR, while Al^{3+} functions as an adsorption site that facilitates substrate enrichment (Fig. 5a). Benefiting from the synergistic interplay between these active and adsorption sites, the catalyst exhibited significantly higher HMFOR activity than either $Al(OH)_3$ or $Co(OH)_2$ alone, achieving nearly 100% HMF conversion and FE (Fig. 5b). Building on the advantages of composite hydroxides, subsequent studies have advanced toward bimetallic hydroxides, which offer additional flexibility in tuning electronic structures and redox properties. Among them, LDHs have emerged as particularly promising candidates due to their well-defined layered architecture and tunable metal composition.[36,76] Yang *et al.* synthesized ultrathin NiFe–LDH and NiMn–LDH catalysts using a formamide-assisted coprecipitation method.[77] *In situ* characterization and theoretical calculations revealed that the intrinsic defect structure of the ultrathin LDHs enhances the deprotonation ability of M–OH sites, weakens the O–H bond covalency, and promotes the formation of high-valent metal species, thereby significantly improving catalytic activity. This finding highlights that the rational regulation of the deprotonation ability is an effective strategy to boost HMFOR performance. Expanding on defect and composition regulation in LDHs, Cheng *et al.* designed a defect-site filling strategy to optimize the surface chemistry of CoFe–LDH catalysts.[18] They first synthesized CoFe–LDH rich in Ov by the hydrothermal method and alkaline etching, and then introduced S atoms to fill these vacancies. The introduction of S reduces the number of Ov and effectively alleviates the strong adsorption effect caused by excess Ov, thereby optimizing and balancing the adsorption behavior of HMF and OH species (Fig. 5c and d). Thanks to this defect-filling strategy, the optimized S–Ov–LDH catalyst maintained approximately 97% FDCA yield and a high FE of approximately 94% after five cycles (Fig. 5e). This strategy provides a new design approach for the structural regulation and performance improvement of electrocatalysts. To further enhance the catalytic activity and durability, researchers have also introduced noble metals onto bimetallic hydroxides, leveraging their strong adsorption capability and high intrinsic activity. For example, Liu *et al.* synthesized NiCo hydroxides by a co-precipitation method, followed by loading Pd nanoclusters to obtain Pd/NiCo.[75] The incorporation of Co modulated the d-orbital structure of Ni, thereby lowering the onset potential for the HMFOR, while Pd exhibited strong adsorption affinity toward HMF molecules, facilitating the interaction between Ni active sites and HMF (Fig. 5f). Benefiting from the synergistic effects of Co and Pd, Pd/NiCo exhibited markedly enhanced catalytic performance, maintaining high yield and FE even after five electrochemical cycles, indicative of its excellent stability (Fig. 5g and h).

4.4 Metal chalcogenides

Metal chalcogenides (mainly sulfides and selenides) have received widespread attention in HMFOR research in recent years.[78] Among them, metal sulfides, represented by nickel sulfide, are considered potential high-efficiency catalysts in the

HMFOR due to their abundant active sites and excellent conductivity.[79,80] However, the activity and selectivity of Ni_3S_2-based catalysts in the HMFOR are still far from satisfactory.[81] Therefore, it is necessary to introduce strategies such as electrochemical reconstruction, heteroatom doping, and synergistic regulation of both from the perspective of electronic structure and interfacial environment control to further improve their catalytic performance. Among these strategies, electrochemical reconstruction, as a dynamic structural evolution mechanism in the reaction process, can induce *in situ* gradual oxidation of the sulfide surface to form oxide species such as NiOOH, thereby significantly altering its interfacial electronic structure and adsorption properties. Xiao *et al.* achieved the electrochemical activation reconstruction of Ni_3S_2 by controlling the concentration of HMF in KOH solution, resulting in a series of Ni_3S_2/NiO_X-*n* catalysts with continuously tunable compositions (Fig. 6a).[82] By adjusting the ratio of Ni_3S_2 to NiO_X, the competitive adsorption between HMF and OH^- could be effectively balanced and optimized. Among them, the Ni_3S_2/NiO_X reconstructed under 15 mM HMF exhibited the highest catalytic activity. Moreover, the Ni_3S_2/NiO_X-15 catalyst exhibits an FDCA FE of up to 98% and retains excellent stability during continuous electrolysis for over 100 hours (Fig. 6b). Unlike *in situ* reconstruction, heteroatom doping optimizes catalytic performance by altering the electronic structure and local coordination environment of Ni_3S_2. Sun *et al.* reported the synthesis of Co-doped Ni_3S_2 on NF, yielding a porous Co_x-NiS@NF catalyst.[81] The porous architecture offers abundant active sites and promotes efficient mass transport. $Co_{0.4}$-NiS@NF delivers outstanding HMFOR performance, reaching 497 mA cm^{-2} at 1.45 V *vs.* RHE, highlighting its promising potential for large-scale electrolytic hydrogen production. Further research shows that introducing Mn can also effectively modulate the electronic environment of Ni-based sulfides. The Mn-doped NiS nanosheets prepared by Li *et al.* maintain over 98% FDCA selectivity and high FE even at an industrial-grade current density of 500 mA cm^{-2} by providing additional Mn–O/Mn–HMF adsorption sites and promoting Ni^{2+}/Ni^{3+} conversion.[80] In addition, the doping-reconstruction synergistic regulation strategy combines the advantages of both, achieving multi-dimensional performance enhancements by simultaneously regulating the local electronic environment and constructing the active phase *in situ*. For example, Xu *et al.* doped Ni_3S_2 with Cu, V, Zn, and Fe elements, respectively, and then restructured the material by electrochemical oxidation (Fig. 6c).[83] Among them, the constructed Cu/Ni_3S_2–R exhibited the best catalytic performance (Fig. 6d). The introduction of Cu modulates the electronic structure of Ni sites, generating more Lewis acid sites, thereby promoting the initial adsorption of HMF. The subsequent electrochemical surface reconstruction generates highly active NiOOH and expands the ECSA, enabling the catalyst to have faster charge transport capabilities and better reaction kinetics in the HMFOR. Ultimately, the Cu/Ni_3S_2–R catalyst achieved nearly 100% FDCA yield and nearly 100% FE (Fig. 6e). Beyond sulfides, selenide systems have also attracted increasing attention. Recently, Liu *et al.* reported a $CoSe_2$@NiSe–$CoSe_2$/NF heterostructure constructed *via* hydrothermal synthesis and a post-selenization step (Fig. 6f).[21] The resulting $CoSe_2$@NiSe–$CoSe_2$/NF heterostructure exhibits superior HMFOR performance compared with $CoSe_2$ and NiSe, requiring only 1.29 V and 1.36 V to achieve 10 and 50 mA cm^{-2}, respectively (Fig. 6g). Moreover, over ten consecutive cycles, the total FE and FDCA yield reached 98.1% and 98.6%, respectively (Fig. 6h).

4.5 Metal phosphides

Metal phosphides exhibit unique advantages in the HMFOR due to their high electrical conductivity and metal–phosphorus synergistic effects.[84] However, pristine metal phosphides often suffer from limited active sites and poor structural stability, making it difficult to achieve ideal catalytic performance. To overcome these challenges, researchers have employed strategies such as heterostructure construction and metal doping to optimize their electronic structure and interfacial properties, thereby significantly enhancing catalytic activity and selectivity. The following section highlights recent advances in representative metal phosphide catalysts and their mechanistic roles in the HMFOR. Fu *et al.* successfully constructed a Ni_3P–Cu_3P heterostructure on a copper foam (CF) substrate.[20] XPS analysis revealed that the Cu 2p peak of Ni_3P–Cu_3P/CF shifted by approximately 0.3 eV toward a lower binding energy compared with Cu_3P/CF, while the Ni 2p peak exhibited a positive shift of about 0.5 eV relative to Ni_3P/CF (Fig. 7a and b). These energy shifts indicate an interfacial electron redistribution, in which electrons transfer from Ni_3P to Cu_3P, thereby inducing the formation of high-valence Ni active species. Meanwhile, the electron-enriched Cu_3P domains effectively suppressed the competing OER process, resulting in a remarkable improvement in both the conversion efficiency and product selectivity of the HMFOR. The Ni_3P–Cu_3P/CF catalyst achieved a HMF conversion of 100%, FDCA selectivity of 99.4%, and FE of 99.2%, significantly outperforming single Ni_3P and Cu_3P catalysts (Fig. 7c). Following a similar interfacial modulation principle, Wang *et al.* designed a CoP–CoOOH heterojunction catalyst.[85] The strong coupling at the CoP/CoOOH interface facilitated directional electron transfer and strengthened reactant adsorption, together resulting in markedly enhanced HMFOR activity. These studies highlight that rational heterostructure construction can simultaneously promote charge redistribution, optimize adsorption energetics, and suppress side reactions. In addition to heterostructure engineering, metal doping provides another powerful approach to modulate the electronic structure in phosphide catalysts. Min *et al.* successfully synthesized Mn-doped CoP catalysts on carbon cloth (Mn_x–CoP/CC) by the hydrothermal method followed by phosphorization.[86] The incorporation of Mn facilitated electron transfer from Co to P, resulting in Co electron depletion and P electron enrichment, while simultaneously accelerating the formation of MnCoOOH. Benefiting from this electronic modulation and surface reconstruction behavior, the catalyst exhibited multifunctional properties, enabling efficient catalysis of the hydrogen evolution reaction (HER) and HMFOR. In summary, heterostructure construction and metal doping

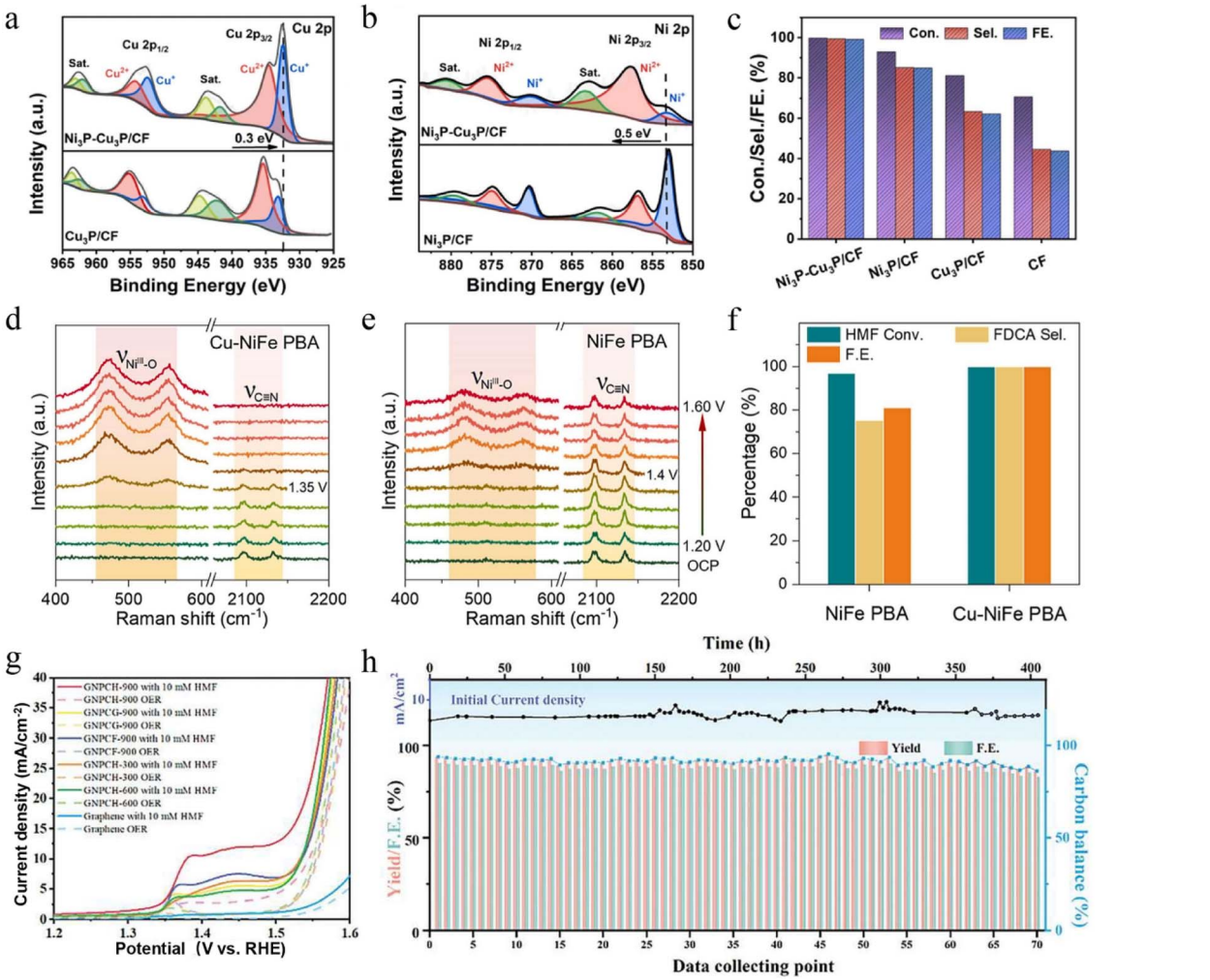

Fig. 7 (a) Cu 2p XPS spectra of Ni_3P–Cu_3P/CF and Cu_3P/CF. (b) Ni 2p XPS spectra of Ni_3P–Cu_3P/CF and Ni_3P/CF. (c) HMF conversion, FDCA selectivity, and FE of Ni_3P–Cu_3P/CF, Ni_3P/CF, Cu_3P/CF, and CF.[20] Copyright 2024, Elsevier. (d and e) *In situ* Raman spectra of Cu–NiFe PBA and NiFe PBA at different potentials. (f) Comparison of HMF conversion, FDCA selectivity, and FE for NiFe PBA and Cu–NiFe PBA.[91] Copyright 2025, Elsevier. (g) LSV curves in 1 M KOH with and without 10 mM HMF. (h) Catalyst recyclability test of GNPCH-900.[92] Copyright 2025, Wiley-VCH GmbH.

synergistically modulate the electronic and surface properties of metal phosphides, greatly enhancing their performance in selective HMFOR.

4.6 Other metal compounds

In addition to the common metal-based catalysts mentioned above, other types of metal-based compounds also show potential for application in the HMFOR.[87] For example, metal nitrides and metal–organic frameworks (MOF) have all demonstrated excellent catalytic performance.[88,89] Although research on these materials is still in the exploratory stage, they offer new insights and research directions for HMFOR catalyst design. Zhou *et al.* successfully constructed a Co_4N@CeO_2 heterostructure on NF by the hydrothermal impregnation method.[90] In this system, CeO_2 extracts electrons from Co_4N, thereby modulating the electronic distribution at the hetero-interface and optimizing the electronic structure of the active sites. The Co_4N@CeO_2/NF exhibits outstanding multifunctional catalytic performance, demonstrating excellent activity in the HER, OER, and HMFOR. Besides, Zhou *et al.* introduced V doping into Ni_3N, which effectively promoted surface reconstruction and generated highly active hydroxide species, thereby markedly enhancing the FDCA yield.[50] In addition to metal nitrides, Liu *et al.* synthesized NiFe Prussian blue analogue (PBA) and Cu–NiFe PBA using a hydrothermal method.[91] *In situ* Raman spectroscopy showed that, compared with NiFe PBA, Cu–NiFe PBA exhibited a significant Ni^{3+}–O vibrational peak at a lower potential (1.35 V), which gradually increased with increasing potential, while its cyano group signal showed a significant attenuation (Fig. 7d and e). Furthermore, Cu^{2+} causes the d-band center of adjacent Ni atoms to shift upward to the Fermi level, thereby enhancing their adsorption capacity for –OH and –CHO in HMF molecules, and thus accelerating the oxidation of HMF to FDCA. Under the combined effects of the above electronic regulations, Cu–NiFe PBA still maintains

Table 1 Summary of the performance of different electrocatalysts for the conversion of HMF to FDCA

Categories	Catalysts	Electrolyte/HMF concentration	E (V *vs.* RHE)	Yied/selectivity (%)	FE (%)	Ref.
Metals/alloys	Ni(NS)/CP	0.1 M KOH/5 mM	1.36	99.4/–	—	61
	Ni@C	1 M KOH/10 mM	1.45	98.2/–	98.5	62
	Pt_1Ni_3	1 M KOH/50 mM	1.45	98/–	98	64
	Ni–Cu	1 M KOH/50 mM	1.45	99.5/100	99.7	15
Metal oxides	Ov–Co_3O_4	1 M KOH/10 mM	1.47	91.9/–	88.1	22
	Pd–$NiCo_2O_4$	1 M KOH/50 mM	1.5	–/99.2	99.6	68
	NF@Co_3O_4/CeO_2	1 M KOH/10 mM	1.40	94.5/–	97.5	69
	CuO–PdO	1 M KOH/50 mM	—	96.2/–	93.7	70
Metal hydroxides	S–Ov–CoFe LDH	1 M KOH/50 mM	—	98.4/–	94.9	18
	Mn–$Ni(OH)_2$/PMS	1 M KOH/50 mM	1.4	99.6/–	98.5	73
	$Al(OH)_3$/$Co(OH)_2$	1 M KOH/10 mM	1.5	99.1/–	99.4	74
	Pd/NiCo hydroxides	1 M KOH/50 mM	—	96.5/–	95.9	75
Metal chalcogenides	$CoSe_2$@NiSe–$CoSe_2$/NF	1 M KOH/10 mM	1.4	98.6/–	98.1	21
	Ni_3S_2/NF	1 M KOH/50 mM	1.4	98.8/–	97.6	79
	$Mn_{0.2}$NiS/GF	1 M KOH/100 mM	—	97.6/98.3	94.2	80
	$Co_{0.4}$NiS@NF	1 M KOH/10 mM	1.45	>99.0/>99.0	99.1	81
	Cu/Ni_3S_2–R	1 M KOH/20 mM	1.4	100/100	100	83
Metal phosphides	Ni_3P–Cu_3P/CF	1 M KOH/10 mM	1.44	–/99.4	99.2	20
	CoP–CoOOH	1 M KOH/150 mM	1.42	–/96.3	96.3	85
	NiFeP	1 M KOH/10 mM	1.435	99.4/99.4	94.6	97
Other metal compounds	NiB_x	1 M KOH/10 mM	1.4	98.8/99.0	99.5	42
	V–Ni_3N	1 M KOH/10 mM	1.475	>95.4/98.2	98.2	50
	Cu–NiFe PBA	1 M KOH/100 mM	—	–/99.8	99.7	91
Metal-free catalysts	GNPCH-900	1 M KOH/10 mM	1.446	>90.0/>90.0	>90.0	92

excellent catalytic performance even under high-concentration HMF conditions. It achieves nearly 100% HMF conversion, 99.8% FDCA selectivity, and 99.7% FE, demonstrating its strong potential for industrial application (Fig. 7f). These findings indicate that many more metal-based materials with unique structures and electronic properties remain to be discovered, offering broad opportunities for future advancements in HMFOR catalysis.

4.7 Metal-free catalysts

Metal-free materials featuring low cost, high conductivity, tunable physicochemical properties, and excellent stability are potential catalysts for various electrochemical transformations.[93–95] In recent years, research on metal-freecatalysts for the HMFOR has gradually become an important direction in the field of biomass conversion. Current research focuses on solving the problems of high cost, resource scarcity, and environmental burden of traditional precious metal or transition metal catalysts, and improving catalytic efficiency and stability through innovative design. Although the research on metal-free catalytic systems directly targeting the HMFOR is still relatively limited, the progress in related fields has provided potential paths and inspiration for this direction. In 2019, Qin *et al.* prepared N and B co-doped porous carbon materials.[96] The metal-free electrocatalyst was used for the HMFOR, and the HMF conversion rate reached 71% and the FDCA yield was 57%. This work provides new and in-depth insights into the rational design and activity origin of metal-free electrocatalysts, and also makes it possible to explore further applications of HMFOR metal-free catalysts. Moreover, the establishment of structure–function relationships also provides a theoretical basis for the design of metal-free catalysts for the HMFOR. Wang and his colleagues reported that graphene-like nitrogen-doped porous carbon sheets (GNPCH) are highly efficient metal-free electrocatalysts for HMFOR.[92] As illustrated in Fig. 7g and h, the GNPCH pyrolyzed at 900 °C (GNPCH-900) shows a substantially lower onset potential for the HMFOR than the other catalysts, accompanied by a markedly enhanced current density. More importantly, the reaction can proceed continuously for over 400 hours, during which both the final FDCA yield and the FE remain above 90%. These findings not only elucidate the structure–activity relationship between the catalyst's microstructure and its performance but also offer valuable insights for the future development and design of metal-free HMFOR catalysts.

In summary, diverse classes of electrocatalysts have been developed for the HMFOR, each presenting distinct advantages and limitations. Table 1 provides a comparative overview of the catalytic performance of representative electrocatalysts. Metals and alloys possess high intrinsic activity but are often limited by corrosion and instability in oxidative environments, requiring conductive supports and structural modulation. Conversely, metal oxides and hydroxides (*e.g.*, Co, Ni, and Fe-based) feature tunable redox chemistry and abundant active sites but suffer from low conductivity, often necessitating defect engineering or doping. Chalcogenides and phosphides benefit from high conductivity and synergistic effects, delivering excellent FDCA yields and FE, typically after *in situ* surface reconstruction. Emerging candidates like nitrides, MOFs, and metal-free catalysts expand design possibilities yet face hurdles regarding

activity, durability, and mechanistic clarity. Despite progress, common challenges persist, including managing adsorption/desorption energies, suppressing the competitive OER, and ensuring stability at industrial current densities. Overall, integrating compositional regulation, electronic structure tuning, and interfacial engineering is essential to bridge the gap between fundamental studies and practical HMFOR applications.

5 Reaction conditions

The electrochemical conversion of HMF is subject to several sources of uncertainty, including the intrinsic instability of the substrate, the presence of impurities in the electrolyte, and the analytical challenges associated with product quantification.[29,98] Rigorous accounting for these factors is essential to ensure the reliability and accuracy of electrochemical evaluations. Crucially, these uncertainties are not isolated; they are inextricably coupled with the fundamental parameters of the electrolyte system—specifically pH, composition, and applied potential.[27,38,99]

Electrolyte pH governs the reaction pathway by modulating the adsorption behavior and dissociation states of both HMF and its intermediates.[100] Simultaneously, the applied potential establishes the thermodynamic driving force for electron transfer, directly dictating product distribution and selectivity. Furthermore, the electrolyte composition, particularly the identity of supporting ions, introduces specific interactions that can alter interfacial properties and reaction kinetics. Consequently, the systematic and synergistic control of pH, composition, and potential is imperative for achieving reproducible, accurate, and comparable assessments of HMF electroconversion processes.

5.1 Electrolyte pH

The electrolyte pH serves as a determining factor in the thermodynamics and kinetics of the HMFOR electrocatalytic reaction.[101,102] The HMFOR reaction pathway involves multiple intermediates, and under different pH conditions, the reaction follows distinct pathways. This is due to the different adsorption properties and reactivity of the aldehyde and hydroxyl groups at varying pH levels.[26] Under mild alkaline or neutral conditions (pH < 13), the oxidation of the $-CH_2OH$ group is favored, leading to the DFF pathway. In contrast, under strong alkaline conditions (pH $\geq$ 13), the oxidation of the –CHO group predominates, promoting the HMFCA pathway. The pH of the electrolyte modulates the selectivity of the reaction pathway and the formation of intermediates, thereby influencing the distribution of the final products.[32] In general, the electrooxidation of HMF to FDCA can proceed under acidic, neutral, and alkaline conditions. However, acidic and neutral environments often lead to limited catalytic activity and lower product selectivity due to sluggish reaction kinetics and instability of the catalyst. In contrast, under alkaline conditions, most reported electrocatalysts can readily achieve high FDCA yields and FE. Therefore, the current research on the HMFOR mainly focuses on the electrooxidation of HMF under alkaline conditions. Alkaline electrolytes have become the main reaction medium for the electrocatalytic HMFOR due to their unique catalytic advantages.[22,103] Zeng and co-workers designed and prepared nanoporous mesh-type NiFe layered double hydroxides (Rh-SA/NiFe NMLDH) as a highly active and stable alkaline HMFOR catalyst.[104] It is worth noting that Rh-SA/NiFe NMLDH has top catalytic activity for the HMFOR, with an onset potential of 1.2 V *vs.* RHE, an extremely low potential of 1.3 V *vs.* RHE at 50 mA cm^{-2}, an FE close to 100%, and excellent long-term stability. Prajapati *et al.* studied the effect of electrolyte pH on the HMFOR by varying the pH of the electrolyte.[105] As shown in Fig. 8a, the HMFOR showed different activity and selectivity trends between high alkaline and low alkaline environments, with high activity for the HMFOR and high selectivity for FDCA at pH = 13, and low HMFOR activity and high selectivity for DFF at pH = 11. These pH-dependent variations in product selectivity highlight the dynamic interplay between competing reaction pathways, emphasizing the critical role of electrolyte pH in determining reaction outcomes. However, it has been reported that under alkaline conditions, the formation of aldehyde intermediates can be suppressed due to the facile hydration of aldehydes into geminal diols, which are less reactive.[106,107] So some researchers have explored the use of neutral electrolytes to modulate the reaction pathway. In fact, in neutral media, the oxidation of the aldehyde group in HMF can be significantly inhibited, thereby favoring the accumulation of intermediate products such as DFF.[108] This highlights that a neutral pH environment may facilitate the selective synthesis and stabilization of aldehyde-containing intermediates during the HMFOR.[16] Ge and co-workers reported using single-atom ruthenium on nickel oxide (Ru_1–NiO) as a catalyst to selectively produce aldehydes in the neutral medium.[16] As illustrated in Fig. 8b, DFF emerges as the predominant product within the investigated potential range, suggesting that the oxidation of hydroxyl groups constitutes the most favorable reaction pathway for the HMFOR under neutral pH conditions. Ru_1–NiO also exhibited a low potential of 1.283 V *vs.* RHE at 10 mA cm^{-2}, and a DFF selectivity of 90%. It reveals that the neutral electrolyte plays an important role in achieving high aldehyde selectivity. In addition, He *et al.* designed and synthesized an S–Ru/MnO_2 amorphous structure catalyst and combined it with an electrochemical pulse method to promote the electroconversion of HMF to FDCA in a neutral electrolyte, achieving a 100% HMF conversion rate and a 98.7% FDCA yield at a current density of 47 mA cm^{-2}.[109] Alkaline electrolytes have been widely employed in the HMFOR due to their ability to significantly enhance the efficiency of FDCA production. However, at the industrial scale, large quantities of acid and base are required to adjust the pH for FDCA precipitation and recovery, which substantially increases production costs. In contrast, performing HMFOR in acidic electrolytes allows for the efficient separation of FDCA *via in situ* crystallization or solvent extraction, without the need for pH adjustment. Zhang *et al.* prepared MnO_2-modified carbon electrodes *via* an electrodeposition process, resulting in a carbon electrode hereafter referred to as ε-MnO_2.[110] The ε-MnO_2-modified carbon electrode was subsequently subjected to thermal treatment, and the resulting electrode was designated as ε-MnO_2/b. Thereafter, ε-MnO_2/b was

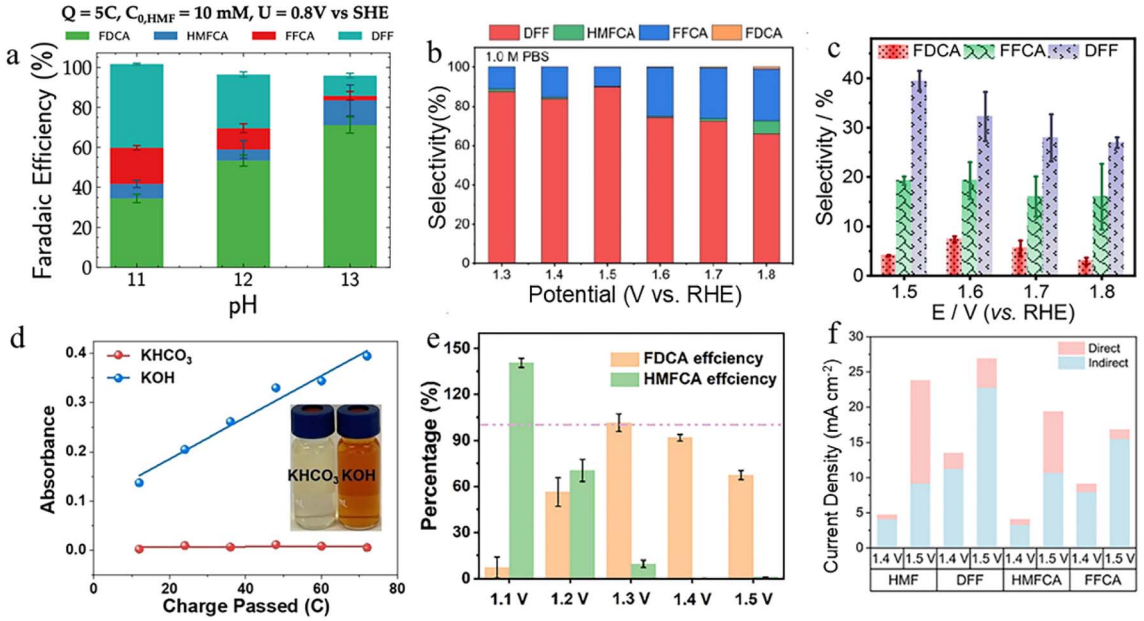

Fig. 8 (a) Product distribution at different pH levels of the HMFOR on a thin-film nickel catalyst.[105] Copyright 2024, American Chemical Society. (b) Product distribution at different potentials over Ru_1–NiO in 1.0 M PBS after passing 10 C charge.[16] Copyright 2022, Wiley-VCH GmbH. (c) The different product selectivities of ε-MnO_2/bp in 0.5 M H_2SO_4 with 50 mM HMF.[110] Copyright 2025, The Royal Society of Chemistry. (d) Ultraviolet-visible spectroscopy spectra of anodized HMF electrolytes in 1 M $KHCO_3$ and 1 M KOH, respectively.[114] Copyright 2024, Wiley-VCH GmbH. (e) FE of FDCA and HMFCA of the Ag–$Co(OH)_2$ sample at different potentials.[116] Copyright 2024, Wiley-VCH GmbH. (f) Current component due to Cu^{3+}-mediated DOP and IOP of HMF, HMFCA, DFF, and FFCA at 1.4 and 1.5 V.[117] Copyright 2025, Wiley-VCH GmbH.

employed as the working electrode and underwent chronopotentiometric pretreatment, yielding the final electrode, referred to as ε-MnO_2/bp, and then their electrocatalytic activities for the HMFOR were evaluated. Fig. 8c illustrates the changes in product selectivity as the voltage varies. It was found that the ε-MnO_2/bp catalyst exhibited the best electrocatalytic oxidation performance, with a conversion rate of 92.95% and a yield of FDCA of 23.03% under the conditions of 60 °C, 0.5 M H_2SO_4, and 1.6 V *vs.* RHE. This strategy offers a promising approach for establishing a sustainable, low-carbon, and energy-efficient process for the continuous production of FDCA.[111] In summary, the electrolyte pH critically influences both the activity and selectivity of the HMFOR process. The HMF conversion, FDCA yield, and FE during the HMFOR process can be effectively regulated by tuning the electrolyte's pH.

5.2 Electrolyte composition

The selection of electrolyte plays a pivotal role in governing the performance of the HMFOR, including activity, selectivity, and stability, by modulating the interfacial reaction environment, dictating the reaction pathway, and affecting the state of the catalyst.[112] The most commonly used electrolyte is KOH, with a concentration of usually 1 M, which provides a high concentration of OH^- and usually has a high reaction activity. Choi *et al.* synthesized a NiP/$Ni(PO_3)_2$/$NiMoO_4$ hybrid (SR_P-NMO) containing Ov by the double ion leaching method and carried out the HMFOR process in a 1.0 M KOH electrolyte solution.[113] The results showed that it had significant catalytic efficiency at a low potential of 1.37 V and obtained a FDCA yield of up to 97.4% in a short reaction time. Some researchers also used weak acid salts as electrolytes. Compared with strong bases, it has better buffering properties and can reduce the influence of local pH changes;[114] it has lower corrosiveness; and it may slightly improve selectivity or stability in some systems. Lei *et al.* synthesized a pCoHA-Ru catalyst consisting of ultra-dense RuO_x clusters supported on a cobalt hydroxide-based support.[114] Anodic oxidation of the HMF-containing electrolyte under two distinct pH conditions results in a marked difference in solution color, with absorbance varying by 1.0 to 2.0 orders of magnitude, and the solution is almost clear under the $KHCO_3$ electrolyte with 0.1 M HMF (Fig. 8d). Without undergoing a large amount of polymerization, pCoHA-Ru exhibited superior performance in a 1 M $KHCO_3$ electrolyte solution (pH = 8.31), effectively converting HMF into FFCA and FDCA with a yield of 92.1%, providing a new route for the two-step conversion of HMF while greatly reducing polymerization. Lee and colleagues proposed the selection of a combination of triethylamine (TEA) and carbonate as the anolyte to replace the traditional KOH electrolyte, enabling the HMFOR in the paired electrolysis system to operate stably for a long time under mild pH conditions.[115] The use of TEA provides a suitable pH value, preventing alkali-induced HMF degradation while maintaining a stable anolyte pH value, because the protons produced in the alcohol/aldehyde oxidation reaction are chelated by TEA. The addition of carbonate to TEA promotes the electrochemical oxidation of alcohol to aldehyde by interacting with the hydroxyl protons of the alcohol group. These improvements enabled stable FDCA production for 150 hours during HMF electrolysis, maintaining

initial performance without electrolyte replacement. These results highlight the importance of optimizing the anolyte composition for long-term, reliable electrolysis. In summary, the choice of electrolyte significantly influences the HMFOR. Different electrolyte types, due to differences in their acid–base properties, ionic radius, charge density, and coordination and adsorption capacity, directly alter the dominant reaction pathway and influence the state of catalytically active sites, thereby regulating reaction rate, product selectivity, and overall efficiency.

5.3 Potential

Potential has a significant effect on the HMFOR process. In general, high potential will trigger the OER, reducing the yield and FE of FDCA. At a lower potential, the HMFOR process mainly produces DFF and HMFCA intermediates, while the production of FDCA requires a higher potential.[112] Therefore, how to achieve high current density in a limited potential range is the key to the success of the HMFOR.[45] Moreover, by precisely tuning the applied potential to influence the pathway selectivity of the HMFOR, selective generation of diverse products can be achieved under different potential conditions. Zhou and his colleagues constructed Ag–$Co(OH)_2$ heterogeneous catalysts and used the tandem synergistic catalytic effect of the composite catalysts to electrocatalyze the HMF oxidation reaction in an alkaline electrolyte solution, greatly reducing the reaction potential of the HMFOR (1.03 V *vs.* RHE).[116] Furthermore, as shown in Fig. 8e, the combined FE of HMFCA and FDCA at potentials below 1.3 V *vs.* RHE exceeded 100%, indicating that the non-faradaic reaction was a Cannizzaro reaction catalyzed by Ag. At the same time, the reaction was carried out at different potentials. The HMFCA yield was 91.3% at 1.1 V *vs.* RHE, and the FDCA yield was 92.8% at 1.4 V *vs.* RHE. The highly efficient and selective synthesis of HMFCA and FDCA across different potential ranges was achieved. This work demonstrates the selective synthesis of two high-value-added chemicals using a tandem catalyst, providing powerful guidance for the design and development of efficient multi-component catalysts. Tong *et al.* reported the growth of CuO_xH_y on Cu foam as a model electrocatalyst to investigate the active phases of the Cu-based catalyst in the HMFOR.[117] Fig. 8f shows that for HMF and HMFCA, the indirect oxidation current (I_{ind}) dominates at 1.4 V *vs.* RHE, while the contribution of the direct oxidation current (I_d) increases significantly at 1.5 V *vs.* RHE. Conversely, DFF and FFCA display a consistently dominant I_{ind} at both 1.4 and 1.5 V *vs.* RHE. All results show that at potentials below 1.4 V *vs.* RHE, CuO exhibits a relatively low HMFOR activity, with the reaction primarily proceeding through the Cu^{2+}-mediated direct oxidation process (DOP). When the potential is increased to approximately 1.5 V *vs.* RHE, the Cu^{3+}-mediated direct oxidation process becomes activated, where the high surface coverage of the catalyst primarily hinders the adsorption of –CHO, while the increased potential primarily promotes the adsorption and subsequent oxidation of –OH, reversing the selectivity. In a word, the active sites of the catalysts and their adsorption behavior toward organic substrates can be tuned by adjusting the applied potential, ultimately achieving selective product formation. These findings facilitate the rational design of more efficient electrocatalysts for the selective and value-added conversion of biomass.

6 Summary and prospects

This review outlines the reaction pathway and mechanism of the HMFOR, elucidating the key steps involved and their inherent challenges, laying the theoretical foundation for subsequent content. Recent mechanistic studies have focused on core issues such as the equilibrium adsorption of HMF and OH^-, and the rapid conversion of high-valence active species (*e.g.*, Ni^{2+}/Ni^{3+}). Standard evaluation methods are then summarized to provide a reference for benchmarking and the rational optimization of catalyst performance. Next, various catalyst systems are systematically discussed, with a focus on strategies and mechanisms for improving activity and selectivity. Overall, catalyst development has primarily focused on Ni, Co, and Fe-based systems, with defect engineering, heteroatom doping, heterostructure construction, and dynamic surface reconstruction becoming widely effective and transferable design strategies applicable to different catalyst types. Furthermore, there is a growing recognition that reaction conditions (including pH, electrolyte composition, and potential) play a crucial role in determining reaction pathways and product selectivity, reflecting a shift from materials-centric design to holistic reaction system regulation. Given the significant gap between current laboratory research findings and industrial application needs, this review concludes by summarizing the key issues that urgently need to be addressed and proposing possible future development directions, aiming to promote efficient and scalable FDCA electrosynthesis.

6.1 Standardized evaluation protocols

Currently, significant discrepancies exist across research groups regarding electrolyte composition, catalyst loading, operating parameters, and performance metrics.[118] This lack of unified standards hinders the rigorous comparative benchmarking of catalyst performance. Consequently, there is an urgent need to establish a standardized and universal testing protocol. For instance, under alkaline conditions, a consensus standard could be adopted: a three-electrode system using 1 M KOH containing 10 mM HMF, a scan rate of 5 mV s^{-1}, and 90% *iR* compensation, with performance normalized to mass activity. Such a standardized framework would not only facilitate valid comparisons among different HMFOR catalysts but also significantly enhance the reproducibility of research findings.

6.2 In-depth mechanistic studies

Despite significant progress in HMFOR research, the complete catalytic mechanism remains to be fully elucidated. Specifically, there is limited understanding regarding the dynamic surface reconstruction of catalysts and the evolution of active sites under operating conditions, which obscures the identity of the true catalytic centers. Furthermore, a systematic correlation

linking catalyst composition, geometric structure, and electronic configuration to activity has yet to be fully established. Consequently, future research must integrate advanced *in situ*/*operando* characterization with theoretical simulations. This approach is essential for tracking the evolution of key intermediates and revealing intrinsic active sites, thereby providing a profound understanding of the reaction mechanism. Such efforts will facilitate the development of a comprehensive structure–activity relationship framework, offering a solid theoretical basis for the rational design and optimization of efficient catalytic systems.

6.3 Exploration of field-assisted catalysis

Beyond intrinsic material properties such as composition and structure, external physical fields (*e.g.*, light, thermal, magnetic, or strain fields) play a pivotal role in modulating local electronic structures, intermediate adsorption energies, and reaction pathways. Leveraging these effects offers additional degrees of freedom for tuning catalytic selectivity and activity without altering the bulk composition of the catalyst.[119,120] While field effects have been validated in other electrochemical systems, their application in the HMFOR remains nascent and largely unexplored. Future research in this direction could unveil new paradigms for controllable and high-efficiency biomass valorization.

6.4 Multifunctional catalysts for coupled systems

Coupling the HMFOR with reductive half-reactions, such as the HER or carbon dioxide reduction reaction (CO_2RR), enables the concurrent production of high-value chemicals and clean energy.[30,90] However, to overcome the efficiency bottlenecks and high costs associated with conventional paired electrolysis, the rational design of bifunctional or multifunctional catalysts is imperative. This strategy enhances overall energy efficiency by integrating anodic and cathodic functionalities into a single system. Despite the clear potential of this approach, significant challenges persist regarding catalyst durability and the kinetic balancing of paired reactions. Addressing these issues is critical for advancing the practical application of the HMFOR in integrated renewable energy and chemical synthesis systems.

6.5 Expanding the electrolyte pH scope

Alkaline media are preferred in the HMFOR due to their superior reaction kinetics, offering high concentrations of OH^- species and low reaction barriers. However, alkaline systems suffer from increased process complexity due to post-reaction acidification and purification. In contrast, acidic media facilitate product separation and integration with biomass hydrolysis but suffer from severe catalyst corrosion and side reactions, leading to reduced reaction efficiency and selectivity. Consequently, expanding the applicable electrolyte pH range and identifying optimal pH windows that balance reaction kinetics and catalyst stability are essential for improving HMFOR efficiency. Neutral or mildly acidic environments may represent an effective compromise, mitigating corrosion and suppressing competing reactions while preserving favorable reaction kinetics. Accordingly, the development of acid-stable catalysts, enabled by strategies such as carbon encapsulation, metal doping, and surface modification, is critical for achieving pH-flexible HMFOR operation.

6.6 Data-driven catalyst discovery and rational design

The multidimensional complexity of the HMFOR renders traditional trial-and-error approaches inefficient. Artificial intelligence (AI) and machine learning (ML) offer a very promising solution for catalyst design, capable of unraveling complex structure–activity relationships. In the synthesis, characterization, and application of catalytic materials in catalytic processes, ML techniques not only provide new avenues for catalyst design but also offer powerful tools for a deeper understanding of the relationship between material properties and catalytic activity. This knowledge helps establish principles for designing catalysts and improving their efficiency. Future research should prioritize identifying universal "descriptors" for high-throughput screening and advancing inverse design to computationally generate optimal structures based on performance targets. Ultimately, coupling AI-driven predictions with automated robotic platforms (*i.e.*, "closed-loop" systems) promises to dramatically accelerate the catalyst discovery cycle from years to months.

6.7 Synergistic reactor design and interface engineering

Transitioning from *H*-type cells to continuous flow and membrane electrode assembly (MEA) reactors is essential for industrial viability.[121–123] The configuration, material choice, and structural refinement of electrolytic devices are critical in modulating the electrode–electrolyte interface, a factor that dictates reaction efficiency, stability, and long-term sustainability. In continuous flow and MEA systems, the optimization of cell components has led to substantial improvements in both stability and current density. Beyond merely enhancing reaction rates, advancements in reactor engineering contribute to extended system lifespans and superior operational reliability. Advanced reactors not only optimize reactant-catalyst mass transport but also provide precise control over temperature and pressure, effectively suppressing undesirable side reactions. Consequently, the continued evolution of reactor technology plays an indispensable role in the industrial implementation of the HMFOR. To overcome mass transport limitations and gas accumulation at high currents, a multi-scale strategy is required: microscopically, by modulating wettability and local pH to optimize diffusion; and macroscopically, by refining fluid dynamics to minimize ohmic losses. Integrating these interfacial controls with robust reactor design is key to achieving sustained, ampere-level current densities.

6.8 Bridging the gap to industrial implementation

Commercialization hinges on bridging the gap between ideal lab conditions and realistic industrial environments. A critical challenge is ensuring catalyst robustness against impurities (*e.g.*, humins and lignin) found in crude hydrolysates, which often poison active sites. Future work must prioritize materials

with intrinsic tolerance to these "dirty" feedstocks. Furthermore, as techno–economic viability is dictated by downstream processing, developing integrated "reaction–separation" technologies is imperative. The ultimate goal is to deliver holistic solutions that achieve high efficiency, industrial-grade durability (>1000 hours), and simplified recovery to ensure economic feasibility.

Author contributions

Jiacheng Zhang: visualization, investigation & writing-original draft. Siping Wang: visualization, investigation & writing-original draft. Jiaqing Liu: visualization. Jiayi Chen: writing-review & editing. Guigang Zhang: writing-review & editing. Yidong Hou: writing-review & editing. Meifang Zheng: supervision, writing-review & editing. Sibo Wang: supervision, writing-review & editing. Xue Feng Lu: conceptualization, supervision, writing-review & editing.

Conflicts of interest

The authors declare no conflicts of interest.

Data availability

The data supporting this article have been included.

Acknowledgements

This work was supported by the National Natural Science Foundation of China (22409028 and 22472031) and Fujian Province Minjiang Scholar Program (XRC-24084).

References

1 D. J. Davidson and J. Andrews, Not all about consumption, *Science*, 2013, **339**, 1286–1287.
2 M. Song, X. Yang, C. Guo, S. Zhang, J. Ma and H. Gao, Nanoflower $Mn_xNi_{2-x}P$ as efficient bifunctional catalyst for hydrogen production with urea-assisted energy-saving in alkaline freshwater and seawater, *EcoEnergy*, 2025, **3**, 470–481.
3 M. Wang, H. Zhou and F. Wang, Photocatalytic biomass conversion for hydrogen and renewable carbon-based chemicals, *Joule*, 2024, **8**, 604–621.
4 J. Li, X. Hao, J. Zhao, J. Li, B. Su, Z. Ding, M. Huang, Z. Lan, M. Yang and S. Wang, Light-induced electronic structure modulation in perovskite ferrite for efficient photothermal dry reforming of methane, *Chem. Sci.*, 2026, DOI: 10.1039/d5sc05708f.
5 H. Fan, X. Bu, Z. Wan, S. Sun, H. Lou, X. Zhou, J. Gao, J. Miao, J. Zhang, W. Gao and D. Wen, Adsorption-mediated efficient glucose electrooxidation on transition metal aerogels for biomass upgradation, *Chem. Sci.*, 2025, **16**, 21094–21103.
6 H. Wu, J. Song, H. Liu, Z. Xie, C. Xie, Y. Hu, X. Huang, M. Hua and B. Han, An electrocatalytic route for transformation of biomass-derived furfural into 5-hydroxy-2(5H)-furanone, *Chem. Sci.*, 2019, **10**, 4692–4698.
7 C. Xu, E. Paone, D. Rodríguez-Padrón, R. Luque and F. Mauriello, Recent catalytic routes for the preparation and the upgrading of biomass derived furfural and 5-hydroxymethylfurfural, *Chem. Soc. Rev.*, 2020, **49**, 4273–4306.
8 C. Chen, M. Lv, H. Hu, L. Huai, B. Zhu, S. Fan, Q. Wang and J. Zhang, 5-Hydroxymethylfurfural and its downstream chemicals: a review of catalytic routes, *Adv. Mater.*, 2024, **36**, 2311464.
9 B. Wozniak, S. Tin and J. G. de Vries, Bio-based building blocks from 5-hydroxymethylfurfural via 1-hydroxyhexane-2,5-dione as intermediate, *Chem. Sci.*, 2019, **10**, 6024–6034.
10 D. Chen, W. Li, J. Liu and L. Sun, Bio-inspired proton relay for promoting continuous 5-hydroxymethylfurfural electrooxidation in a flowing system, *Energy Environ. Sci.*, 2025, **18**, 3120–3128.
11 C. Wang, Y. Wu, A. Bodach, M. L. Krebs, W. Schuhmann and F. Schüth, A novel electrode for value-generating anode reactions in water electrolyzers at industrial current densities, *Angew. Chem., Int. Ed.*, 2022, **62**, e202215804.
12 L. Zhuang, W. Cai, H. Ji, Q. Li, G. Wang, S. Xin, Q. Zhao, F. Cheng, Y. Guo, L. Mao, Y. Tian, F. Wu, L. Zhang, Y. Xiang, J. Hu, R. Cao, L. Xiao, H. Tao, W. Xing, D. Zhan, H. Liao, M. Xiao, B. Ren, Z. Peng, R. Wen, X. Wang, Y. Song, H. Lü, B. Xia, G. Wang, J. Cheng, Z. Liu, M. Zhou, B. Huang, C. Li, Y. Zou, S. Wang, H. Lin and Z. Wei, Development trends and priority research fields of electrochemical discipline in the 15th five year plan period, *J. Electrochem.*, 2025, **31**, 2510081.
13 D. Si, X. Teng, B. Xiong, L. Chen and J. Shi, Electrocatalytic functional group conversion-based carbon resource upgrading, *Chem. Sci.*, 2024, **15**, 6269–6284.
14 H. Wang and J. Lu, Brief introduction of organic electrochemistry, *J. Electrochem.*, 2011, **17**, 366–372.
15 D. Chen, Y. Ding, X. Cao, L. Wang, H. Lee, G. Lin, W. Li, G. Ding and L. Sun, Highly efficient biomass upgrading by a Ni–Cu electrocatalyst featuring passivation of water oxidation activity, *Angew. Chem., Int. Ed.*, 2023, **62**, e202309478.
16 R. Ge, Y. Wang, Z. Li, M. Xu, S. M. Xu, H. Zhou, K. Ji, F. Chen, J. Zhou and H. Duan, Selective electrooxidation of biomass-derived alcohols to aldehydes in a neutral medium: promoted water dissociation over a nickel-oxide-supported ruthenium single-atom catalyst, *Angew. Chem., Int. Ed.*, 2022, **61**, e202200211.
17 H. Wang, Y. Song, X. Liu, S. Lu, C. Zhou, Y. Jin and Y. Yang, Preparation of anisotropic MnO_2 nanocatalysts for selective oxidation of benzyl alcohol and 5-hydroxymethylfurfural, *Trans. Tianjin Univ.*, 2020, **26**, 382–390.
18 B. Cheng, H. Zhan, Y. Lu, D. Xing, X. Lv, T. Frauenheim, P. Zhou, S. Wang and Y. Zou, Oxygen defect site filling strategy induced moderate enrichment of reactants for efficient electrocatalytic biomass upgrading, *Adv. Sci.*, 2024, **11**, 2410725.

19 C. Liu, X. R. Shi, K. Yue, P. Wang, K. Zhan, X. Wang, B. Y. Xia and Y. Yan, S-species-evoked high-valence $Ni^{2+\delta}$ of the evolved β-$Ni(OH)_2$ electrode for selective oxidation of 5-hydroxymethylfurfural, *Adv. Mater.*, 2023, **35**, 2211177.
20 J. Fu, G. Yang, Y. Jiao, C. Tian, H. Yan and H. Fu, Ni-Cu-based phosphide heterojunction for 5-hydroxymethylfurfural electrooxidation-assisted hydrogen production at large current density, *Nano Energy*, 2024, **127**, 109727.
21 S. Liu, W. Cai, M. Jin, T. Zhang, Z. Zhang, Q. Liu, X. Liu, X. Zhang and F. Wang, $CoSe_2$@NiSe-$CoSe_2$ heterojunction for enhanced electrocatalytic 5-hydroxymethylfurfural oxidation coupled with hydrogen evolution, *Adv. Funct. Mater.*, 2025, **35**, 2421447.
22 Y. Lu, T. Liu, C. Dong, C. Yang, L. Zhou, Y. Huang, Y. Li, B. Zhou, Y. Zou and S. Wang, Tailoring competitive adsorption sites by oxygen-vacancy on cobalt oxides to enhance the electrooxidation of biomass, *Adv. Mater.*, 2021, **34**, 2107185.
23 P. Zhu, M. Shi, Z. Shen, X. Liao and Y. Chen, Electrocatalytic conversion of biomass-derived furan compounds: mechanisms, catalysts and perspectives, *Chem. Sci.*, 2024, **15**, 4723–4756.
24 L. Chen and Y. Liu, Advances and prospects of selective electrocatalytic upgrading of 5-hydroxymethylfurfural to furan-2,5-dicarboxylic acid, *Chem. Rec.*, 2025, **25**, e202400238.
25 H. Dong, H. Li, F. Ye and Y. Fang, Quantitative kinetic and catalytic analysis of 5-hydroxymethylfurfural electrooxidation reaction through in-situ Raman spectroscopy, *Chem. Eng. J.*, 2025, **514**, 162518.
26 X. Jiang, W. Li, Y. Liu, L. Zhao, Z. Chen, L. Zhang, Y. Zhang and S. Yun, Electrocatalytic oxidation of 5-hydroxymethylfurfural for sustainable 2,5-furandicarboxylic acid production—from mechanism to catalysts design, *SusMat*, 2023, **3**, 21–43.
27 L. Guo, X. Zhang, L. Gan, L. Pan, C. Shi, Z. F. Huang, X. Zhang and J. J. Zou, Advances in selective electrochemical oxidation of 5-hydroxymethylfurfural to produce high-value chemicals, *Adv. Sci.*, 2023, **10**, 2205540.
28 M. Guo, X. Lu, J. Xiong, R. Zhang, X. Li, Y. Qiao, N. Ji and Z. Yu, Alloy-driven efficient electrocatalytic oxidation of biomass-derived 5-hydroxymethylfurfural towards 2,5-furandicarboxylic acid: a review, *ChemSusChem*, 2022, **15**, e202201074.
29 L. Chen, C. Yu, X. Song, J. Dong, J. Mu and J. Qiu, Integrated electrochemical and chemical system for ampere-level production of terephthalic acid alternatives and hydrogen, *Nat. Commun.*, 2024, **15**, 8072.
30 J. Zhang, D. Yan, G. Ding, X. Wang, C. Li, S. Zhong, Y. Yu, L. Shuai and G. Liao, Dual Co sites in n-n type heterojunction enable selective electrochemical Co-valorization of HMF and CO_2, *Angew. Chem., Int. Ed.*, 2025, **64**, e202511448.
31 N. Zhang, Y. Zou, L. Tao, W. Chen, L. Zhou, Z. Liu, B. Zhou, G. Huang, H. Lin and S. Wang, Electrochemical oxidation of 5-Hydroxymethylfurfural on nickel nitride/carbon nanosheets: reaction pathway determined by in situ sum frequency generation vibrational spectroscopy, *Angew. Chem., Int. Ed.*, 2019, **58**, 15895–15903.
32 X. Liu, J. Tang, Y. Chen, X. Song, J. Guo, G. Wang, S. Han, X. Chen, C. Zhang, S. Dou, H. Shao and D. Wang, Refining electrocatalyst design for 5-hydroxymethylfurfural oxidation: insights into electrooxidation mechanisms, structure–property correlations, and optimization strategies, *ACS Catal.*, 2025, **15**, 7308–7339.
33 Y. Fan, H. Zhao, J. Wang, W. Li, F. Wei, M. Liu, Y. Yu, F. Yu, W. Lu and G. Zhang, Critical practices in improving the electrochemical oxidation of 5-hydroxymethylfurfural to 2,5-furandicarboxylic acid in 0.1 M KOH, *ACS Sustain. Chem. Eng.*, 2024, **12**, 3256–3264.
34 Y. Yang, D. Xu, B. Zhang, Z. Xue and T. Mu, Substrate molecule adsorption energy: An activity descriptor for electrochemical oxidation of 5-hydroxymethylfurfural (HMF), *Chem. Eng. J.*, 2022, **433**, 133842.
35 Y. Yang and T. Mu, Electrochemical oxidation of biomass derived 5-hydroxymethylfurfural (HMF): pathway, mechanism, catalysts and coupling reactions, *Green Chem.*, 2021, **23**, 4228–4254.
36 M. Zhang, Y. Liu, B. Liu, Z. Chen, H. Xu and K. Yan, Trimetallic NiCoFe-layered double hydroxides nanosheets efficient for oxygen evolution and highly selective oxidation of biomass-derived 5-hydroxymethylfurfural, *ACS Catal.*, 2020, **10**, 5179–5189.
37 M. T. Bender, Y. C. Lam, S. Hammes-Schiffer and K.-S. Choi, Unraveling two pathways for electrochemical alcohol and aldehyde oxidation on NiOOH, *J. Am. Chem. Soc.*, 2020, **142**, 21538–21547.
38 B. J. Taitt, D. Nam and K. Choi, A comparative study of nickel, cobalt, and iron oxyhydroxide anodes for the electrochemical oxidation of 5-hydroxymethylfurfural to 2,5-furandicarboxylic acid, *ACS Catal.*, 2018, **9**, 660–670.
39 G. Liu, T. Nie, Z. Song, X. Sun, T. Shen, S. Bai, T. Yu, L. Zheng and Y. F. Song, Pd-embedded NiFe layered double hydroxides for biomass upgrading: precision construction of dual-functional synergistic sites, *Adv. Funct. Mater.*, 2024, **34**, 2411284.
40 Z. Yang, B. Zhang, C. Yan, Z. Xue and T. Mu, The pivot to achieve high current density for biomass electrooxidation: Accelerating the reduction of Ni^{3+} to Ni^{2+}, *Appl. Catal., B*, 2023, **330**, 122590.
41 A. C. Cardiel, B. J. Taitt and K.-S. Choi, Stabilities, regeneration pathways, and electrocatalytic properties of nitroxyl radicals for the electrochemical oxidation of 5-Hydroxymethylfurfural, *ACS Sustain. Chem. Eng.*, 2019, **7**, 11138–11149.
42 P. Zhang, X. Sheng, X. Chen, Z. Fang, J. Jiang, M. Wang, F. Li, L. Fan, Y. Ren, B. Zhang, B. J. J. Timmer, M. S. G. Ahlquist and L. Sun, Paired electrocatalytic oxygenation and hydrogenation of organic substrates with water as the oxygen and hydrogen source, *Angew. Chem., Int. Ed.*, 2019, **131**, 9253–9257.

43 W. Xie, Y. Zhang, H. Zheng, P. Lyu, X. Ke, T. Li, H. Fang, Y. Sun, J. Dong, L. Lin, C. Wang and X. Tang, Unlocking the production of biomass-derived plastic monomer 2,5-furandicarboxylic acid at industrial-level concentration, *ACS Catal.*, 2024, **14**, 17510–17524.

44 N. Heidary and N. Kornienko, Electrochemical biomass valorization on gold-metal oxide nanoscale heterojunctions enables investigation of both catalyst and reaction dynamics with operando surface-enhanced Raman spectroscopy, *Chem. Sci.*, 2020, **11**, 1798–1806.

45 Z. Yang, S. Wang, C. Wei, L. Chen, Z. Xue and T. Mu, Proton transfer mediator for boosting the current density of biomass electrooxidation to the ampere level, *Energy Environ. Sci.*, 2024, **17**, 1603–1611.

46 S. Yang, Y. Guo, P. Zhao, H. Jiang, H. Shen, Z. Chen, L. Jiang, X. Xue, Q. Zhang and H. Zhang, Unraveling the electrooxidation mechanism of 5-(hydroxymethyl)furfural at a molecular level via nickel-based two-dimensional metal–organic frameworks catalysts, *ACS Catal.*, 2023, **14**, 449–462.

47 O. van der Heijden, S. Park, R. E. Vos, J. J. J. Eggebeen and M. T. M. Koper, Tafel slope plot as a tool to analyze electrocatalytic reactions, *ACS Energy Lett.*, 2024, **9**, 1871–1879.

48 Y. Shen, H. Deng, Y. C. Huang, P. Du, H. Zhou, M. Ma, A. Shen, M. Wang, C. L. Dong, L. Xu and S. Shen, Promoted electrochemical reconstruction of glassy metal–organic frameworks for efficient electrocatalytic 5-hydroxymethylfurfural oxidation, *Adv. Energy Mater.*, 2024, **15**, 2405364.

49 S. Anantharaj, P. E. Karthik and S. Noda, The significance of properly reporting turnover frequency in electrocatalysis research, *Angew. Chem., Int. Ed.*, 2021, **60**, 23051–23067.

50 Q. Zhou, J. Wang, G. Jin, H. Liu and C. Wang, Enhanced surface reconstruction of V-doped Ni_3N driven by strong OH adsorption to boost 5-hydroxymethylfurfural electrooxidation for energy-saving H_2 production, *J. Mater. Chem. A*, 2024, **12**, 12475–12486.

51 S. S. Jeon, P. W. Kang, M. Klingenhof, H. Lee, F. Dionigi and P. Strasser, Active surface area and intrinsic catalytic oxygen evolution reactivity of NiFe LDH at reactive electrode potentials using capacitances, *ACS Catal.*, 2023, **13**, 1186–1196.

52 D. M. Morales and M. Risch, Seven steps to reliable cyclic voltammetry measurements for the determination of double layer capacitance, *J. Phys.: Energy*, 2021, **3**, 034013.

53 H. Zhu, Y. Liu, W. Guo, J. Zheng, Y. Zheng, S. Cherevko, C. Tang and Q. Zhang, Electrochemical impedance spectroscopy analysis to accelerate electrocatalytic system innovation, *Sci. China: Chem.*, 2024, **67**, 3964–3975.

54 P. Jin, L. Zhang, Z. Wu, B. Zhou, Z. Duan, H. Li, H. Liu, A. Deng, Q. Li, Y. Zhang, C. Zhao and S. Wang, Heterogeneous interface induced Co_3O_4-NiO catalyst for efficient electrocatalytic 5-Hydroxymethylfurfural oxidation, *Chem. Eng. J.*, 2024, **481**, 148303.

55 S. Liao, S. Shi, J. Hu, W. Yao, S. Liu, W. Wang, W. Xiao, D. Zhao, S. Wang and C. Chen, Enhanced electrooxidation of 5-hydroxymethylfurfural over a ZIF-67@β-$Ni(OH)_2$/NF heterostructure catalyst: Synergistic effects and mechanistic insights, *J. Colloid Interface Sci.*, 2025, **688**, 806–817.

56 J. Lei, H. Zhang, J. Yang, J. Ran, J. Ning, H. Wang and Y. Hu, Structural designs and mechanism insights into electrocatalytic oxidation of 5-hydroxymethylfurfural, *J. Energy Chem.*, 2025, **100**, 792–814.

57 P. A. Kempler and A. C. Nielander, Reliable reporting of Faradaic efficiencies for electrocatalysis research, *Nat. Commun.*, 2023, **14**, 1158.

58 S. Geiger, O. Kasian, M. Ledendecker, E. Pizzutilo, A. M. Mingers, W. T. Fu, O. Diaz Morales, Z. Li, T. Oellers, L. Fruchter, A. Ludwig, K. J. J. Mayrhofer, M. T. M. Koper and S. Cherevko, The stability number as a metric for electrocatalyst stability benchmarking, *Nat. Catal.*, 2018, **1**, 508–515.

59 P. Hauke, M. Klingenhof, X. Wang, J. F. de Araújo and P. Strasser, Efficient electrolysis of 5-hydroxymethylfurfural to the biopolymer-precursor furandicarboxylic acid in a zero-gap MEA-type electrolyzer, *Cell Rep. Phys. Sci.*, 2021, **2**, 100650.

60 S. Zhang, Z. Chen, J. F. Gu, W. Sang, M. Jiang, S. Li, P. Wang, Z. Kou and C. Chen, Recent progress in metal-catalyzed selective oxidation of 5-hydroxymethylfurfural into furan-based value-added chemicals, *Chem. Rec.*, 2023, **23**, e202300019.

61 X. Lu, K. H. Wu, B. Zhang, J. Chen, F. Li, B. J. Su, P. Yan, J. M. Chen and W. Qi, Highly efficient electro-reforming of 5-hydroxymethylfurfural on vertically oriented nickel nanosheet/carbon hybrid catalysts: structure–function relationships, *Angew. Chem., Int. Ed.*, 2021, **60**, 14528–14535.

62 Y. Li, K. Alorku, C. Shen, L. Yan, Q. Li, X. Tian, W. Li, Y. Xu, C. Wang, C. Li, L. Ma, H. Duan, Q. Liu and J. Jiang, In-situ redispersion of Ni@C catalyst boosts 5-hydroxymethylfurfural electrooxidation by increasing Ni^{4+} sites, *Appl. Catal., B*, 2024, **357**, 124250.

63 L. Shi, W. Cai, F. Zhang, S. Li, X. Liu, Y. Liu, P. Ren, B. Li, S. Liu and B. Liu, Engineering oxygen intermediates adsorption on amorphous NiFe alloys for highly active and selective electrochemical biomass conversion, *Angew. Chem., Int. Ed.*, 2025, **64**, e202424345.

64 J. Wu, Z. Kong, Y. Li, Y. Lu, P. Zhou, H. Wang, L. Xu, S. Wang and Y. Zou, Unveiling the adsorption behavior and redox properties of PtNi nanowire for biomass-derived molecules electrooxidation, *ACS Nano*, 2022, **16**, 21518–21526.

65 L. Zhang, P. Jin, Z. Wu, B. Zhou, J. Jiang, A. Deng, Q. Li, T. Hussain, Y. Zhang, H. Liu and S. Wang, CuO/Co_3O_4 bifunctional catalysts for electrocatalytic 5-hydroxymethylfurfural oxidation coupled cathodic ammonia production, *Energy Environ. Mater.*, 2024, **7**, e12725.

66 Y. Wang, H. He, H. Lv, F. Jia and B. Liu, Two-dimensional single-crystalline mesoporous high-entropy oxide

nanoplates for efficient electrochemical biomass upgrading, *Nat. Commun.*, 2024, **15**, 6761.
67 Y. Lu, T. Liu, C. Dong, Y. Huang, Y. Li, J. Chen, Y. Zou and S. Wang, Tuning the selective adsorption site of biomass on Co_3O_4 by Ir single atoms for electrosynthesis, *Adv. Mater.*, 2021, **33**, 2007056.
68 X. Jiang, X. Ma, Y. Yang, Y. Liu, Y. Liu, L. Zhao, P. Wang, Y. Zhang, Y. Lin and Y. Wei, Enhancing the electrocatalytic oxidation of 5-hydroxymethylfurfural through cascade structure tuning for highly stable biomass upgrading, *Nano-Micro Lett.*, 2024, **16**, 275.
69 G. Zhao, G. Hai, P. Zhou, Z. Liu, Y. Zhang, B. Peng, W. Xia, X. Huang and G. Wang, Electrochemical oxidation of 5-hydroxymethylfurfural on CeO_2-modified Co_3O_4 with regulated intermediate adsorption and promoted charge transfer, *Adv. Funct. Mater.*, 2023, **33**, 2213170.
70 P. Zhou, X. Lv, S. Tao, J. Wu, H. Wang, X. Wei, T. Wang, B. Zhou, Y. Lu, T. Frauenheim, X. Fu, S. Wang and Y. Zou, Heterogeneous-interface-enhanced adsorption of organic and hydroxyl for biomass electrooxidation, *Adv. Mater.*, 2022, **34**, 2204089.
71 G. Grabowski, J. Lewkowski and R. Skowroński, The electrochemical oxidation of 5-hydroxymethylfurfural with the nickel oxide/hydroxide electrode, *Electrochim. Acta*, 1991, **36**, 1995.
72 Z. Yang, L. Chen, Y. Yin, C. Wei, Z. Xue and T. Mu, Weakened hydrogen bond connectivity promotes interfacial mass transfer for industrial level scalable biomass electrooxidation, *Energy Environ. Sci.*, 2024, **17**, 8801–8809.
73 L. Chen, Z. Yang, Q. Hu, C. Yan, Y. Yao, Y. Bao, Z. Pei, T. Mu and Z. Xue, Engineering gradient d-d orbital occupancy to boost substrate adsorption for efficient electrocatalytic biomass valorization, *Angew. Chem., Int. Ed.*, 2025, **64**, e202511868.
74 H. Dai, Y. Huang, H. Bai, H. Li, H. Zhao, F. Wang, W. Fan and W. Shi, Adsorption–activation bifunctional center of Al/Co-base catalyst for boosting 5-hydroxymethylfurfural oxidation, *Adv. Energy Mater.*, 2024, **14**, 2402789.
75 G. Liu, T. Nie, Z. Song, X. Sun, T. Shen, S. Bai, L. Zheng and Y. F. Song, Pd loaded NiCo hydroxides for biomass electrooxidation: understanding the synergistic effect of proton deintercalation and adsorption kinetics, *Angew. Chem., Int. Ed.*, 2023, **62**, e202311696.
76 S. Barwe, J. Weidner, S. Cychy, D. M. Morales, S. Dieckhöfer, D. Hiltrop, J. Masa, M. Muhler and W. Schuhmann, Electrocatalytic oxidation of 5-(hydroxymethyl) furfural using high-surface-area nickel boride, *Angew. Chem., Int. Ed.*, 2018, **57**, 11460–11464.
77 Y. Yang, W. H. Lie, R. R. Unocic, J. A. Yuwono, M. Klingenhof, T. Merzdorf, P. W. Buchheister, M. Kroschel, A. Walker, L. C. Gallington, L. Thomsen, P. V. Kumar, P. Strasser, J. A. Scott and N. M. Bedford, Defect-promoted Ni-based layer double hydroxides with enhanced deprotonation capability for efficient biomass electrooxidation, *Adv. Mater.*, 2023, **35**, 2305573.
78 Z. Fan, Q. Yang, W. Zhang, H. Wen, H. Yuan, J. He, H. G. Yang and Z. Chen, Self-reconstruction of sulfate-terminated copper oxide nanorods for efficient and stable 5-hydroxymethylfurfural electrooxidation, *Nano Lett.*, 2023, **23**, 11314–11322.
79 L. Chen, Z. Yang, C. Yan, Y. Yin, Z. Xue, Y. Yao, S. Wang, F. Sun and T. Mu, Modulating Ni–S coordination in Ni_3S_2 to promote electrocatalytic oxidation of 5-hydroxymethylfurfural at ampere-level current density, *Chem. Sci.*, 2024, **15**, 12047–12057.
80 S. Li, S. Wang, Y. Wang, J. He, K. Li, Y. Xu, M. Wang, S. Zhao, X. Li, X. Zhong and J. Wang, Doped Mn enhanced NiS electrooxidation performance of HMF into FDCA at industrial-level current density, *Adv. Funct. Mater.*, 2023, **33**, 2214488.
81 Y. Sun, J. Wang, Y. Qi, W. Li and C. Wang, Efficient electrooxidation of 5-hydroxymethylfurfural using co-doped Ni_3S_2 catalyst: promising for H_2 production under industrial-level current density, *Adv. Sci.*, 2022, **9**, 2200957.
82 D. Xiao, X. Bao, D. Dai, Y. Gao, S. Si, Z. Wang, Y. Liu, P. Wang, Z. Zheng, H. Cheng, Y. Dai and B. Huang, Boosting the electrochemical 5-hydroxymethylfurfural oxidation by balancing the competitive adsorption of organic and OH^- over controllable reconstructed Ni_3S_2/NiOx, *Adv. Mater.*, 2023, **35**, 2304133.
83 P. Xu, Z. Bao, Y. Zhao, L. Zheng, Z. Lv, X. Shi, H. E. Wang, X. Fang and H. Zheng, Anionic regulation and heteroatom doping of Ni-based electrocatalysts to boost biomass valorization coupled with hydrogen production, *Adv. Energy Mater.*, 2023, **14**, 2303557.
84 S. Xie, H. Fu, L. Chen, Y. Li and K. Shen, Carbon-based nanoarrays embedded with Ce-doped ultrasmall Co_2P nanoparticles enable efficient electrooxidation of 5-hydroxymethylfurfural coupled with hydrogen production, *Sci. China: Chem.*, 2023, **66**, 2141–2152.
85 H. Wang, Y. Zhou and S. Tao, CoP-CoOOH heterojunction with modulating interfacial electronic structure: A robust biomass-upgrading electrocatalyst, *Appl. Catal., B*, 2022, **315**, 121588.
86 S. Min, G. Yang, Y. Jiao, J. Wang, Y. Liu, Z. Chen, H. Yan and H. Fu, Modulation of active sites induced by CoP via Mn doping enables multifunctional electrocatalytic hydrogen evolution, oxygen evolution, and biomass oxidation reactions, *Adv. Funct. Mater.*, 2025, DOI: 10.1002/adfm.202514250.
87 W. Qi, J. Fang, Z. Yang, B. Li, R. Su and Z. He, A low-cost and easily prepared manganese carbonate as an efficient catalyst for aerobic oxidation of 5-hydroxymethylfurfural to 2,5-diformylfuran, *Trans. Tianjin Univ.*, 2018, **24**, 301–307.
88 Y. Wang, J. Ma, X. Cao, S. Chen, L. Dai and J. Zhang, Bionic Mineralization toward scalable MOF films for ampere-level biomass upgrading, *J. Am. Chem. Soc.*, 2023, **145**, 20624–20633.
89 H. G. Xu, X. R. Ning, J. Y. Zhao, H. Y. Lin, H. Q. Fu, S. Wang, Y. Guo, H. Wu, M. Zhu, H. Y. Yuan, P. F. Liu and H. G. Yang, Reactant-induced activation over amorphous metal-

metalloid electrocatalysts for HMF electrooxidation, *Chem*, 2024, **10**, 2147–2169.

90 P. Zhou, G. Hai, G. Zhao, R. Li, X. Huang, Y. Lu and G. Wang, CeO_2 as an "electron pump" to boost the performance of Co_4N in electrocatalytic hydrogen evolution, oxygen evolution and biomass oxidation valorization, *Appl. Catal., B*, 2023, **325**, 122364.

91 Z. Liu, T. Xiao, X. Wu, C. Hu, X. F. Lu, H. Zhang, J. Zhang, X. Bao and P. Yuan, Cu-induced Ni^{3+}-O active sites in prussian blue analogues enable nearly 100 % selective electrooxidation of 5-hydroxymethylfurfural to produce kilogram-scale 2,5-furandicarboxylic acid, *Appl. Catal., B*, 2025, **378**, 125601.

92 C. Wang, Z. Zhao, W. Cao, Y. Peng, M. Song and Y. Wu, A metal-free carbonaceous material for highly efficient and robust electrochemical biomass valorization, *Adv. Funct. Mater.*, 2025, **35**, 2502618.

93 H. Jin, H. Huang, Y. He, X. Feng, S. Wang, L. Dai and J. Wang, Graphene quantum dots supported by graphene nanoribbons with ultrahigh electrocatalytic performance for oxygen reduction, *J. Am. Chem. Soc.*, 2015, **137**, 7588–7591.

94 F. Yu, H. Zhou, Y. Huang, J. Sun, F. Qin, J. Bao, W. A. Goddard, S. Chen and Z. Ren, High-performance bifunctional porous non-noble metal phosphide catalyst for overall water splitting, *Nat. Commun.*, 2018, **9**, 2551.

95 X. Lu, K. Qi, X. Dai, Y. Li, D. Wang, J. Dou and W. Qi, Selective electrooxidation of 5-hydroxymethylfurfural to 5-formyl-furan-2-formic acid on non-metallic polyaniline catalysts: structure–function relationships, *Chem. Sci.*, 2024, **15**, 11043–11052.

96 Q. Qin, T. Heil, J. Schmidt, M. Schmallegger, G. Gescheidt, M. Antonietti and M. Oschatz, Electrochemical fixation of nitrogen and its coupling with biomass valorization with a strongly adsorbing and defect optimized boron–carbon–nitrogen catalyst, *ACS Appl. Energy Mater.*, 2019, **2**, 8359–8365.

97 R. Luo, Y. Li, L. Xing, N. Wang, R. Zhong, Z. Qian, C. Du, G. Yin, Y. Wang and L. Du, A dynamic $Ni(OH)_2$-NiOOH/NiFeP heterojunction enabling high-performance E-upgrading of hydroxymethylfurfural, *Appl. Catal., B*, 2022, **311**, 121357.

98 W. Xue, Y. Liu, X. Ma, J. Ye, X. Bai, J. Zhao and B. Liu, Tuning the equilibrium of excitons and carriers in the (001) plane-exposed bismuth oxyhalide enables efficient selective photocatalytic oxidation of 5-hydroxymethylfurfural, *ACS Catal.*, 2025, **15**, 9621–9632.

99 W. Liu, L. Dang, Z. Xu, H. Yu, S. Jin and G. W. Huber, Electrochemical oxidation of 5-hydroxymethylfurfural with NiFe layered double hydroxide (LDH) nanosheet catalysts, *ACS Catal.*, 2018, **8**, 5533–5541.

100 L. GálvezVázquez, A. Dutta, S. Vesztergom, Z. Szakály, R. Zaugg, A. V. Rudnev and P. Broekmann, HMF electrooxidation on robust nickel-foam catalysts: effect of pH on electrolysis performance, *J. Catal.*, 2025, **450**, 116321.

101 J. N. Hausmann, B. Traynor, R. J. Myers, M. Driess and P. W. Menezes, The pH of aqueous NaOH/KOH solutions: a critical and non-trivial parameter for electrocatalysis, *ACS Energy Lett.*, 2021, **6**, 3567–3571.

102 S. Wang, H. Feng, T. Liu, Y. Deng, M. Zhang, S. Zhao, J. Han and X. Zhang, Theoretical exploration of the origin of alkaline dependence in the oxidation of 5-hydroxymethylfurfural catalyzed by NiO_2H_x, *ACS Catal.*, 2024, **14**, 9860–9869.

103 L. Gao, Z. Liu, J. Ma, L. Zhong, Z. Song, J. Xu, S. Gan, D. Han and L. Niu, NiSe@NiO_x core-shell nanowires as a non-precious electrocatalyst for upgrading 5-hydroxymethylfurfural into 2,5-furandicarboxylic acid, *Appl. Catal., B*, 2020, **261**, 118235.

104 L. Zeng, Y. Chen, M. Sun, Q. Huang, K. Sun, J. Ma, J. Li, H. Tan, M. Li, Y. Pan, Y. Liu, M. Luo, B. Huang and S. Guo, Cooperative Rh-O_5/Ni(Fe) site for efficient biomass upgrading coupled with H_2 production, *J. Am. Chem. Soc.*, 2023, **145**, 17577–17587.

105 A. Prajapati, N. Govindarajan, W. Sun, J. Huang, H. Bemana, J. T. Feaster, S. A. Akhade, N. Kornienko and C. Hahn, Mechanistic insights into the electrochemical oxidation of 5-hydroxymethylfurfural on a thin-film Ni anode, *ACS Catal.*, 2024, **14**, 10122–10131.

106 H. Zhou, Z. Li, S. Xu, L. Lu, M. Xu, K. Ji, R. Ge, Y. Yan, L. Ma, X. Kong, L. Zheng and H. Duan, Selectively upgrading lignin derivatives to carboxylates through electrochemical oxidative C(OH)–C bond cleavage by a Mn-doped cobalt oxyhydroxide catalyst, *Angew. Chem., Int. Ed.*, 2021, **60**, 8976–8982.

107 M. He, Y. Sun and B. Han, Green carbon science: efficient carbon resource processing, utilization, and recycling towards carbon neutrality, *Angew. Chem., Int. Ed.*, 2022, **61**, e202112835.

108 T.-H. Le, T. Vo and C. Chiang, Highly efficient amorphous binary cobalt-cerium metal oxides for selective oxidation of 5-hydroxymethylfurfural to 2,5-diformylfuran, *J. Catal.*, 2021, **404**, 560–569.

109 Y. He, C. Ma, S. Mo, C. Dong, W. Chen, S. Chen, H. Pang, R. Ma, S. Wang and Y. Zou, Unilamellar MnO_2 nanosheets confined Ru-clusters combined with pulse electrocatalysis for biomass electrooxidation in neutral electrolytes, *Sci. Bull.*, 2025, **70**, 193–202.

110 Y. Zhang, Y. Tu, Y. Huo, G. Pan, Q. Zhang, Z. Liu, G. Yang and F. Peng, Electrocatalytic oxidation of 5-hydroxymethylfurfural by MnO_2 with tunable surface oxidation states, *Catal. Sci. Technol.*, 2025, **15**, 3946–3954.

111 Y. Li, X. Wei, S. Han, L. Chen and J. Shi, MnO_2 electrocatalysts coordinating alcohol oxidation for ultra-durable hydrogen and chemical productions in acidic solutions, *Angew. Chem., Int. Ed.*, 2021, **60**, 21464–21472.

112 Y. Gao, L. Ge, H. Xu, K. Davey, Y. Zheng and S. Qiao, Electrocatalytic refinery of biomass-based 5-hydroxymethylfurfural to fine chemicals, *ACS Catal.*, 2023, **13**, 11204–11231.

113 J. Choi, S. Yoo, P. M. Nguyen, E. Lee, H. Shin and Y. J. Hwang, Phase transition kinetics via operando

monitoring electro-oxidation reaction of 5-hydroxymethylfurfural on amorphous nickel oxyhydroxide, *ACS Catal.*, 2025, **15**, 6906–6917.

114 C. Lei, Z. Chen, T. Jiang, S. Wang, W. Du, S. Cha, Y. Hao, R. Wang, X. Cao and M. Gong, Ultra-dense supported ruthenium oxide clusters via directed ion exchange for efficient valorization of 5-hydroxymethylfurfural, *Angew. Chem., Int. Ed.*, 2024, **63**, e202319642.

115 M. Lee, D. H. Won, U. Lee and D. K. Lee, Achieving stable paired electrolysis of captured CO_2 and 5-hydroxymethylfurfural (HMF) via tuning anolyte composition and anode surface, *Adv. Funct. Mater.*, 2025, DOI: 10.1002/adfm.202506183.

116 P. Zhou, X. Lv, H. Huang, B. Cheng, H. Zhan, Y. Lu, T. Frauenheim, S. Wang and Y. Zou, Construction of Ag–$Co(OH)_2$ tandem heterogeneous electrocatalyst induced aldehyde oxidation and the Co-activation of reactants for biomass effective and multi-selective upgrading, *Adv. Mater.*, 2024, **36**, 2312402.

117 G. Tong, K. Zheng, Z. Feng, R. Su, X. Liu, X. Tao, C. Zhang and C. Xu, Unraveling the potential-regulated selectivity of the Cu-based catalyst in 5-hydroxymethylfurfural electro-oxidation, *Angew. Chem., Int. Ed.*, 2025, **64**, e202512175.

118 F. Schäfer, L. Lückemeier and F. Glorius, Improving reproducibility through condition-based sensitivity assessments: application, advancement and prospect, *Chem. Sci.*, 2024, **15**, 14548–14555.

119 Y. Wang, S. Udyavara, M. Neurock and C. D. Frisbie, Field effect modulation of electrocatalytic hydrogen evolution at back-gated two-dimensional MoS_2 electrodes, *Nano Lett.*, 2019, **19**, 6118–6123.

120 C. Chen, H. Jin, P. Wang, X. Sun, M. Jaroniec, Y. Zheng and S. Qiao, Local reaction environment in electrocatalysis, *Chem. Soc. Rev.*, 2024, **53**, 2022–2055.

121 B. Chen, Q. Hou, R. L. Smith, X. Qi and H. Guo, Electrocatalytic oxidation of biomass-derived furans to 2,5-furandicarboxylic acid-a review, *Green Chem.*, 2025, **27**, 8414–8447.

122 M. Yuan, W. Lu, G. Zhang and F. Cao, Alkalization of acetylacetonates: A facile and versatile method to prepare Ni-based hydroxides for the electrochemical production of bio-based 2,5-furandicarboxylic acid, *Chem. Eng. J.*, 2023, **472**, 145149.

123 D. Li, A. R. Motz, C. Bae, C. Fujimoto, G. Yang, F. Zhang, K. E. Ayers and Y. S. Kim, Durability of anion exchange membrane water electrolyzers, *Energy Environ. Sci.*, 2021, **14**, 3393–3419.